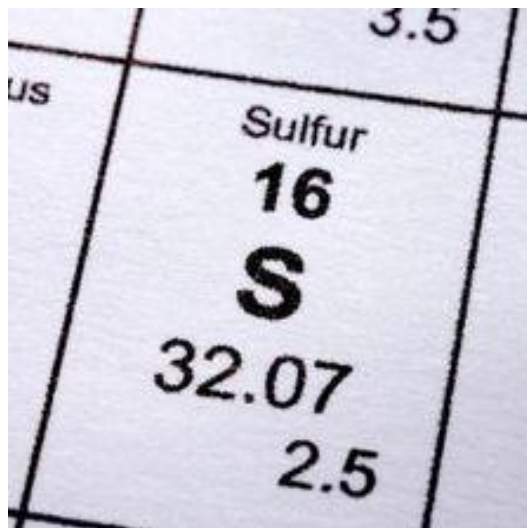


# Effect of Pre-exposure of Sulfur and Iron Sulfide on H<sub>2</sub>S Corrosion at Different Temperatures



Master Thesis  
of  
Brailovskiy Valery



June 2011





Faculty of Science and Technology

## MASTER'S THESIS

|   |  |
|---|--|
| Study program/ Specialization:<br>Masters in Environmental<br>Technology/Offshore   | Spring semester, 2011<br><br>Open                                |
| Writer:<br>Brailovskiy Valery   | .....<br>(Writer's signature)                                    |
| Faculty supervisor: Tor Hemmingsen<br><br>External supervisor(s):   |  |
| Title of thesis:<br><br>Effect of pre-exposure of sulfur and iron sulfide on H <sub>2</sub> S corrosion at different temperatures |  |
| Credits (ECTS): 30  |  |
| Key words:<br><br>Sulfur Deposition<br>H <sub>2</sub> S Corrosion<br>Iron Sulfide<br>Galvanic Corrosion                           | Pages: 68<br><br>+ enclosure: 2 CDs<br><br>Stavanger, 14.06.2011 |



## **ABSTRACT**

The study has been carried out to investigate the effect of elemental sulfur and iron sulfide on corrosion behavior of carbon steel in sour environment. It was found that both compounds could form a protective layer of corrosion products even at low pH and high temperature levels. In general, bare steel electrode behaved as sacrificial anode in two metal galvanic coupling with sulfur or iron sulfide covered steel electrode. However, some examples of opposite behavior were observed in the tests with iron sulfide. The surface of bare steel electrode was coated with a thin black layer and had no evidence of changes due to corrosion. In other hand, surface of sulfur-covered electrode had well adherent thick dark film with traces of pitting. In the case with iron sulfide-covered electrode, the metal surface remained bright with crevice corrosion region.



## **ACKNOWLEDGEMENT**

I would like to express my sincere gratitude to Professor Tor Hemmingsen for his continues academic and moral support.

I would like to thanks my laboratory colleges for priceless advices and moral support too.

Special thanks to my friend Whida Permana.

## TABLE OF CONTENTS

|       |  |    |
|-------|--|----|
| 1     | INTRODUCTION .....                               | 13 |
| 2     | LITERATURE REVIEW .....                          | 14 |
| 2.1   | Sour Environment .....                           | 14 |
| 2.2   | Sour corrosion problems .....                    | 14 |
| 2.3   | Types of corrosion .....                         | 16 |
| 2.4   | Steels used in sour environment .....            | 16 |
| 2.5   | H <sub>2</sub> S Corrosion of carbon steel ..... | 16 |
| 2.5.1 | Presence of elemental S in sour corrosion .....  | 18 |
| 2.5.2 | Effect of temperature and partial pressure ..... | 21 |
| 2.5.3 | Effect of pH .....                               | 21 |
| 2.5.4 | Effect of Cl ions .....                          | 22 |
| 2.5.5 | Effect of concentration H <sub>2</sub> S .....   | 22 |
| 3     | ELECTROCHEMICAL METHODES .....                   | 23 |
| 4     | EXPERIMENTAL PROCEDURE AND SETUP .....           | 25 |
| 4.1   | Research objectives.....                         | 25 |
| 4.2   | Setup.....                                       | 25 |
| 4.3   | Experimental procedures .....                    | 27 |
| 5     | RESULTS AND DISCUSSIONS .....                    | 30 |
| 6     | CONCLUSIONS.....                                 | 59 |
| 7     | RECOMMENDATIONS AND FUTURE WORK.....             | 60 |
|       | REFERENCES.....                                  | 61 |
|       | APPENDIX 1 .....                                 | 65 |
|       | APPENDIX 2 .....                                 | 66 |



## LIST OF FIGURES

|   |    |
|---|----|
| Figure 1. pH at equilibration after mixing water with sulfur at various temperatures. ....  | 20 |
| Figure 2. Effect of NaCl concentration on the corrosion rate of carbon steel in a H <sub>2</sub> O-H <sub>2</sub> S-NaCl system (after Foroulis). ....    | 22 |
| Figure 3. Effect of pH and concentration of H <sub>2</sub> S on corrosion rate. ....  | 23 |
| Figure 4. The galvanic cell.....  | 26 |
| Figure 5. Support for two working and counter electrodes .....  | 27 |
| Figure 6. Galvanic couple between two corroding metals.....   | 31 |
| Figure 7. The OCP values of Fe/Fe+S galvanic couple after 15 minutes and 24 hours at different temperatures (Series 1).....                               | 32 |
| Figure 8. The OCP values of Fe/FeS galvanic couple after 15 minutes and 24 hours at different temperatures.....   | 33 |
| Figure 9. Potentiodynamic sweeps for covered with elemental sulfur working electrode at pH3 at 20°C (blue), 40°C (green), 80°(red) after 15 minutes. .... | 37 |
| Figure 10. Potentiodynamic sweeps for covered with elemental sulfur working electrode at pH7 at 20°C (blue), 40°C (green),80°(red) after 15 minutes.....  | 38 |
| Figure 11. Potentiodynamic sweeps for covered with elemental sulfur working electrode at pH10 at 20°C (blue), 40°C (green),80°(red) after 15 minutes..... | 38 |
| Figure 12. Changes in corrosion current density in time for decoupled sulfur-covered electrode. ....  | 39 |
| Figure 13. Potentiodynamic sweeps for covered with elemental sulfur working electrode at pH3 at 20°C (blue), 40°C (green),80°(red) after 24 hours. ....   | 40 |
| Figure 14. Potentiodynamic sweeps for covered with elemental sulfur working electrode at pH7 at 20°C (blue), 40°C (green),80°(red) after 24 hours. ....   | 40 |
| Figure 15. Potentiodynamic sweeps for covered with elemental sulfur working electrode at pH10 at 20°C (blue), 40°C (green),80°(red) after 24 hours. ....  | 41 |

|   |    |
|---|----|
| Figure 16. Potentiodynamic sweeps for bare working electrode at pH3 at 20°C (blue), 40°C (green), 80° (red) after 24 hours. ....                            | 43 |
| Figure 17. Potentiodynamic sweeps for bare working electrode at pH7 at 20°C (blue), 40°C (green), 80° (red) after 24 hours. ....                            | 43 |
| Figure 18. Potentiodynamic sweeps for bare working electrode at pH10 at 20°C (blue), 40°C (green), after 24 hours. ....                                     | 44 |
| Figure 19. Galvanic corrosion: pH10 at 40°C (blue); pH3 at 40°C (red); pH7 at 80°C (purple); pH10 at 80°C (green); pH3 at 80°C (brown). ....                | 45 |
| Figure 20. Effect of temperature on corrosion rate of the steel [40]. ....  | 46 |
| Figure 21. Surface of bare carbon steel electrode (pH10 at 80°C). ....  | 46 |
| Figure 22. Surface of covered with elemental sulfur carbon steel electrode (pH10 at 80°C). ....   | 47 |
| Figure 23. Picture of covered with Teflon tape and bare working electrodes. ....  | 47 |
| Figure 24. Surface of covered with elemental sulfur electrode (pH10 at 20°C) after removal of Teflon tape. ....   | 48 |
| Figure 25. Potentiodynamic sweeps for covered with iron sulfide working electrode at pH3 at 20°C (blue), 40°C (green), 80° (red) after 15 minutes. ....     | 50 |
| Figure 26. Potentiodynamic sweeps for covered with iron sulfide working electrode at pH7 at 20°C (blue), 40°C (green), 80° (red) after 15 minutes. ....     | 50 |
| Figure 27. Potentiodynamic sweeps for covered with iron sulfide working electrode at pH10 at 20°C (blue), 40°C (green), 80° (red) after 15 minutes. ....    | 51 |
| Figure 28. Changes in corrosion current density in time for decoupled iron sulfide- covered electrode. ....   | 51 |
| Figure 29. Potentiodynamic sweeps for covered with elemental sulfur working electrode at pH3 at 20°C (blue), 40°C (green), 80°C (red) after 24 hours. ....  | 53 |
| Figure 30. Potentiodynamic sweeps for covered with elemental sulfur working electrode at pH7 at 20°C (blue), 40°C (green), 80°C (red) after 24 hours. ....  | 53 |
| Figure 31. Potentiodynamic sweeps for covered with elemental sulfur working electrode at pH10 at 20°C (blue), 40°C (green), 80°C (red) after 24 hours. .... | 54 |

Figure 32. Potentiodynamic sweeps for bare working electrode at pH3 at 20°C (blue), 40°C (green), 80°(red) after 24 hours..... 55

Figure 33. Galvanic corrosion scans for Fe/FeS couple in Series 2. .... 55

Figure 34. Surface of bare carbon steel electrode at pH7 at 80°C. .... 57

Figure 35. Surface of covered (FeS) electrode at pH7 at 80°C after black film has been removed. .... 57

## LIST OF TABLES

|  |    |
|--|----|
| Table 1. The Experimental test matrix .....  | 25 |
| Table 2. Chemical composition of carbon steel X65 (from certificate).....                    | 25 |
| Table 3. The experiments with the covered working electrodes .....                           | 27 |
| Table 4. Potential before and after decoupling of electrodes .....                           | 30 |
| Table 5. Evaluation of the open circuit potential of decoupled electrodes during tests. .... | 35 |
| Table 6. Comparison of Ecorr potential for decoupled electrodes.....                         | 42 |
| Table 7. Galvanic current for covered electrode in coupling Fe/Fe+S ( $\mu\text{A}$ ). ....  | 45 |
| Table 8. Galvanic current for covered electrode in coupling Fe/FeS ( $\mu\text{A}$ ). ....   | 56 |

## 1 INTRODUCTION

The number of sour ( $\text{CO}_2 + \text{H}_2\text{S}$  containing) oil and gas fields being produced worldwide is increasing. As sweet ( $\text{CO}_2$  containing) fields are being depleted, and higher oil prices made it possible for profitable development of sour oil and gas fields [1].

Carbon steel is extensively used in oil and gas pipelines due to low cost. Since long ago companies faced with a corrosion problems related to using the carbon steel tubing in extremely environments which could cause to serious damages in structure. Sulfide stress cracking (SSC) can occur when  $\text{H}_2\text{S}$  is present in the reservoir and is in contact with high-strength steel commonly used in drilling, completing and production wells [2]. For SSC to occur, a metal must be exposed to hydrogen sulfide and under operating conditions conducive to SSC. The critical operating conditions to be considered are if the metal is exposed and, if so, what is the partial pressure of hydrogen sulfide, pH of the water handled, temperature and stress level [3].

Iron sulfide scale formed on internal surfaces of carbon steel tubing and pipelines can be very protective, but localized corrosion attack may occur in the presence of high chloride levels, elemental sulfur or exposure to stagnant water. The formation of iron sulfides is complicated by existence of several stable and metastable Fe-S compounds. Many studies have appeared in the literature; however, no systematic investigation has been reported on the influence of pH and  $\text{H}_2\text{S}$  concentration on the active dissolution of iron in acidic solutions [4]. For understanding of behavior and morphology of sulfides films need more time and more complicated equipment.

The objective of the present work was to study corrosion of carbon steel X65 in solutions of various pH levels and temperatures using potentiostatic polarization methods.

## **2 LITERATURE REVIEW**

### **2.1 Sour Environment**

The number of sour oil and gas fields worldwide is increasing, as sweet fields are being depleted and high oil prices vouch for profitable development of sour oil and gas finds. Sour oil and gas production and transport always imply a risk of material damage and shutdowns due to CO<sub>2</sub>/H<sub>2</sub>S corrosion, and especially localized corrosion attacks.

The NACE Standard MR0175-88 [5] can be used as guidelines for defining a sour environment for the general selection of carbon steel and alloy steels. This definition states that the 0.05-psia (0.34 kPa) H<sub>2</sub>S partial pressure in the gas phase distinguishes SSC failures from no failures in susceptible carbon and low-alloy steels [6].

### **2.2 Sour corrosion problems**

H<sub>2</sub>S is a compound toxic to life that can be associated to natural gas, oil and production water. It is very dangerous to operational staff and causes corrosion cracking and pitting. The generation mechanism of H<sub>2</sub>S has been classified as biotic (biological sources) or abiotic (geological or geochemical sources). The biotic is related to sulfite reducing bacteria (SRB) in reservoirs. Abiotic mechanism involved only chemical reaction between organic, inorganic phases and water. In that case temperature and pressure are critical parameters: thermochemical sulphate reduction (TSR), hydrolysis of metallic sulfurs, cracking or organic compounds, cracking or kerogen and volcanogenic sources are examples of abiotic mechanism [7].

H<sub>2</sub>S is associated with corrosion damage and contributes to several forms of environmental embrittlement. These forms of embrittlement include internal hydrogen blistering, hydrogen induced cracking (HIC) and stress oriented hydrogen induced cracking (SOHIC) of carbon steel plate and pipe material and sulfide stress cracking (SSC) in high strength steels or hard weld zones. It can also

contribute to SSC, hydrogen embrittlement cracking (HEC), localized corrosion and anodic SCC alloys.

**Sulfide Stress Cracking (SSC)** occurs under the combined action of tensile stress and aqueous environments containing H<sub>2</sub>S. This type of cracking occurs at hard martensitic or bainitic areas associated with welds, including both the weld deposit and the heat affected zones. Atomic hydrogen liberated by H<sub>2</sub>S diffuses through the steel and tends to accumulate at areas of high metal hardness and high tensile stress. This mechanism does not require the recombination of hydrogen to molecules and is most often associated with atomic hydrogen. This phenomenon embrittles the steel. The SSC cracks are perpendicular to the tensile stress direction.

During **Hydrogen Induced Cracking (HIC) or stepwise cracking**, hydrogen absorbed from the solution diffuses in the metal and then recombines as hydrogen molecules at trap sites in the steel matrix. High hydrogen pressure can be developed and cracks can initiate. As more hydrogen enters the voids the pressure rises, deforming the surrounding steel so that blisters may become visible at the surface. The steel around the crack becomes highly strained and this can cause linking of adjacent cracks to form stepwise cracking.

**Stress Oriented Hydrogen Induced Cracking (SOHIC)** could be described as combination of HIC and SSC. In SOHIC staggered small cracks are formed approximately perpendicular to the principal stress (applied or residual) resulting in a “ladder-like” crack array. The mode of cracking can be categorized as SSC caused by a combination of external stress and the local straining around hydrogen induced cracks. SOHIC usually occurs in the base metal, adjacent to the HAZ of a weld (where there are high residual stresses from welding) or in a hard weld heat affected zone [8].

As mentioned earlier, the biological source of sour corrosion is SRB causes to Microbial Induced Corrosion (MIC). MIC is very aggressive form of corrosion with many proposes mechanism. Rapid pitting attack can quickly lead to equipment

failure. SRB present in anaerobic layer formed on the metal surface can be detected at corrosion sites in the field by presence of the sulphide films.

### **2.3 Types of corrosion**

Many upstream oil and gas facilities consist of carbon steel pipeline and piping exposed to CO<sub>2</sub> and H<sub>2</sub>S acid gases. Field experience shows that failure of these linens is typically localized/pitting corrosion rather than general corrosion over the entire material surface [9, 10], when the metal loss from the surface. During the localized/pitting corrosion the metal loss is randomly located on the metal surface and anodic sites are formed where the iron sulfides scale could damage. Also corrosion could occur at places with gaskets, bolts and lap joints where crevice exists. Crevice corrosion creates pits similar to pitting corrosion.

### **2.4 Steels used in sour environment**

Carbon steels are generally used for the petroleum industry for transportation of crude oils and gasses from offshore to different refining platforms and from their different destination of the applications. Usually the carbon steel is susceptible to internal corrosion due to CO<sub>2</sub>/H<sub>2</sub>S environment. General principles for selection materials selection and corrosion protection described in NORSOK standard M-011 [11]. The selection of materials shall be optimized and provide acceptable safety and reliability. Steels grades alloyed with high contents of Chromium (Cr), Molybdenum (Mo) and Nickel (Ni) are able to effectively resist corrosion.

### **2.5 H<sub>2</sub>S Corrosion of carbon steel**

Several researches have investigated the corrosion of carbon steel in the presence of H<sub>2</sub>S. The chemistry of H<sub>2</sub>S-H<sub>2</sub>O system is fairly complex. The stability of the different sulfur species present (H<sub>2</sub>S, HS<sup>-</sup> or S<sup>2-</sup>) depends on the solution pH and the redox potential. The corrosion of carbon steel in H<sub>2</sub>S media is influenced by the formation of salts of iron with sulfur anions. The types of iron sulfide scales that are formed include kansite (Fe<sub>9</sub>S<sub>8</sub>), troilite (FeS), pyrrhotite



(Fe<sub>1-x</sub>S), mackinawite (Fe<sub>1+x</sub>S), markasite FeS<sub>2</sub> (S-deficient) and pyrite FeS<sub>2</sub> (S or Fe deficient) [12].

The overall H<sub>2</sub>S corrosion reaction for Fe in an aqueous medium is written as



In most cases, the formation of iron sulfide films (Fe<sub>x</sub>S<sub>y</sub>) on the steel surface becomes the rate-limiting step in H<sub>2</sub>S corrosion. Both the corrosion rate and morphology are intimately related to the electronic, chemical and even mechanical properties of these films. The complex chemistry and mechanism of Fe<sub>x</sub>S<sub>y</sub> formation make this sound like a difficult proposal for experimental investigations. Depending on the environment chemistry and the prior state of the underlying metal, a variety of iron sulfides can be formed. Mackinawite is one of the most prevalent Fe<sub>x</sub>S<sub>y</sub> compounds encountered in slightly sour conditions. Its crystalline structure consists of a tetragonal sulfur-deficient iron sulfide (FeS<sub>1-x</sub>). Due to its (thermodynamic) semistability, mackinawite usually forms as a precursor to some other structures. The semiconductive properties of nonstoichiometric iron sulfides stem from the presence of native point defects. These properties are anticipated to play a crucial role in localized sour corrosion mechanism [13].

In the literature a number of schemes which represent mechanisms of iron sulfide scales formation could be found. In accordance with these studies it is possible to conclude that in the reaction time of first hour very thin sulfide film, possibly mackinawite, forms rapidly on the steel electrode. Based on it the mechanisms of H<sub>2</sub>S corrosion could be described as follows:

1. H<sub>2</sub>S diffuses to the steel surface,
2. H<sub>2</sub>S reacts with the steel to form mackinawite scale on the surface,
3. Mackinawite scale dissolves to Fe(HS)<sup>+</sup> and HS<sup>-</sup>,
4. Fe(HS)<sup>+</sup> diffuses away from the steel surface, and

5. More H<sub>2</sub>S diffuses to react with the exposed steel.

When more ferrous ions were released from the steel surface, cubic ferrous sulfide and troilite precipitated on the steel surface because of high local supersaturation of iron sulfide. If oxygen was involved in the system, it may form thiospinel greigite on the steel surface. At very high concentration of H<sub>2</sub>S, pyrrhotite, marcasite, and pyrite may form on the steel surface [14].

These scales may or may not be protective depending on the conditions such as temperature, pH and H<sub>2</sub>S concentration.

Many studies were carried out to investigate how these parameters affect on corrosion rate.

### **2.5.1 Presence of elemental S in sour corrosion**

Elemental sulfur deposition commonly occurs in production fields with sour environment, especially in high H<sub>2</sub>S concentration level reservoirs. In aqueous conditions, contact of solid sulfur with mild steel can initiate catastrophic corrosion problems. Corrosion process may be dramatically accelerated in the presence of high concentration of salt [15].

The chemical species H<sub>2</sub>S, CO<sub>2</sub> and S of the gas phase as well as the Cl of the brine play a key role on the corrosiveness of the downhole environment. The impact of elemental sulfur is controlled by three main parameters temperature, pressure and the composition of the sour gas, where the H<sub>2</sub>S content has the most significant effect on the S solubility.

From several studies it could be summarized that, S<sub>8</sub> deposition has three predominant potential behavior pathways to consider: chemical reactions, condensate formation, and desublimation of sulfur. The chemical reaction theory, however, can hardly quantify the solid sulfur deposition which takes place immediately with pressure decreased. Condensate formation may lead to the S<sub>8</sub> deposit since liquid hydrocarbons are able to dissolve a part of the vaporized sulfur and evaporation of these condensed liquids results in deposition of sulfur particles. This condensate mechanism is possible only when the gas is

rich in heavy hydrocarbons. Desublimation is the direct transformation of a vapor compound into a solid. As vapor phase becomes saturated, further decreases in either pressure or temperature will instigate a thermodynamic instability, leading to the occurrence of sulfur precipitation via a phase change. Furthermore, condensate formation is a temperature-dominant process whereas desublimation is pressure-dominant. In general, gas transmission systems with a great flow rate have a low temperature drop rate on account of thermal insulation whereas a high pressure drop rate is anticipated under the turbulent flow. Unless the system has a sudden temperature quench locally, the pressure drop rate appears to be a key parameter on elucidating the mechanism of  $S_8$  deposition. Hence, desublimation is the most likely  $S_8$  deposition mechanism [16].

Based on the investigations of several researches the S/H<sub>2</sub>S corrosion can be summarized as follows [17, 18-20].

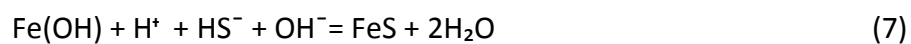
The elemental sulfur dissolves in sour gases and forms various polysulfide species under high temperatures [21]:



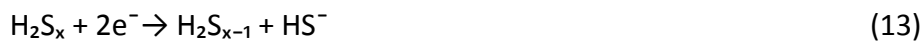
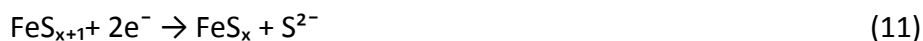
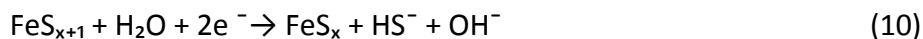
The anodic metal dissolution reactions:



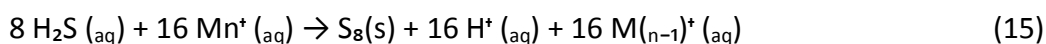
Chemical formation of iron sulfides:



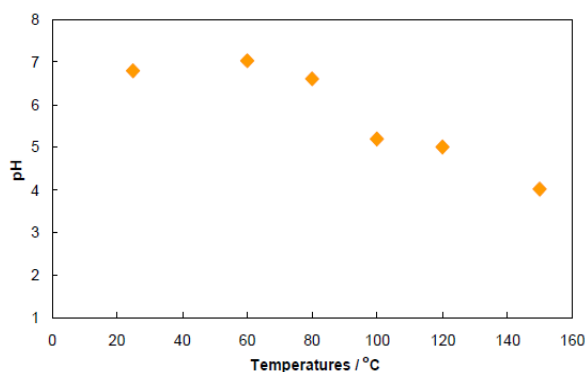
The cathodic reactions:



Elemental sulfur can readily form in aqueous systems via the oxidation of sulfide species [22]. Possible reactions for the formation of elemental sulfur ( $\text{S}_8$ ) could involve high oxidation state metals (denoted  $\text{Mn}^+$ ) or oxygen:



The presence of elemental sulfur could also cause significant acidification of water upon exposure at temperatures in excess of  $80^\circ\text{C}$ . Figure 1 shows the pH at equilibration after mixing with sulfur at various temperatures.



**Figure 1.** pH at equilibration after mixing water with sulfur at various temperatures [23].

### **2.5.2 Effect of temperature and partial pressure**

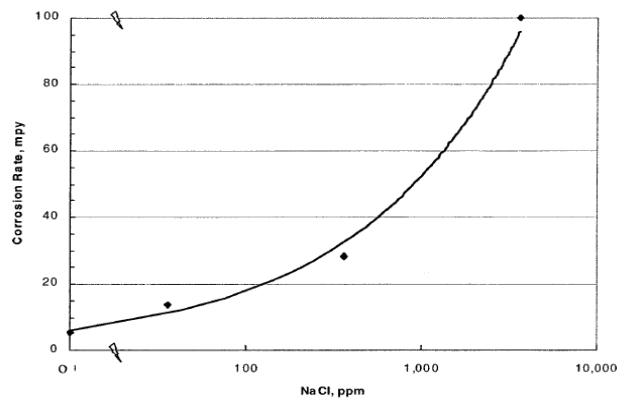
Temperature and partial pressure directly affected the morphology and composition of corrosion products, which in turn caused the change of corrosion rate and occurrence of localized corrosion [24]. But this effect much depends on the exposure time. Hence, the temperature dependence of H<sub>2</sub>S corrosion is very weak for short term exposure and does not seem to have an effect at longer exposure times. This suggests that the corrosion rate is predominantly controlled by the presence of iron sulfide scale [25]. Increasing the temperature and H<sub>2</sub>S concentration increase the sulfidation rate. It is typical that a temperature increase of 50°C will double the sulfidation rate, while increasing the H<sub>2</sub>S concentration by a factor of 10 may be needed to double the sulfidation rate. Therefore, changes of H<sub>2</sub>S concentration are generally less significant, in terms of influencing corrosion, than temperature variations [26]. As the concentration of H<sub>2</sub>S increases, the film formed is rather loose even at pH 3-5 and does not contribute to the corrosion inhibiting effect [27]. With the pressure and temperature drop the solubility of sulfur is decreased and sulfur is deposited when the solubility limit is exceeded.

### **2.5.3 Effect of pH**

The protective nature and composition of the corrosion product depend greatly on the pH of the solution. At lower values of pH (<2), iron is dissolved and iron sulfide is not precipitated on the surface of the metal due to a very high solubility of iron sulfide phases at pH values less than 2. In this case, H<sub>2</sub>S exhibits only the accelerating effect on the dissolution of iron. At pH values from 3 to 5, inhibitive effect of H<sub>2</sub>S is seen due to the formation of ferrous sulfide (FeS) protective film on the electrode surface [28].

#### 2.5.4 Effect of Cl ions

The effect of chloride concentration on the corrosion rate of carbon steel in solutions saturated with H<sub>2</sub>S (at room temperature) is shown in Figure 2. An increase in the chloride concentration, in the range 0 to 3.6% NaCl, increased the corrosion rate exponentially, suggested that the chloride ions inhibit the formation of the sulfide films as well as increase the conductivity of the solution, and, thereby, accelerate corrosion [28].



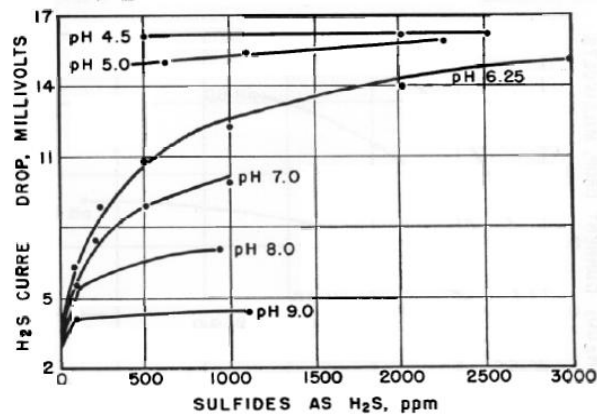
**Figure 2.** Effect of NaCl concentration on the corrosion rate of carbon steel in a H<sub>2</sub>O-H<sub>2</sub>S-NaCl system (after Foroulis) [28].

#### 2.5.5 Effect of concentration H<sub>2</sub>S

The corrosion rate of X65 increases with the increase of H<sub>2</sub>S concentration and decreases with the increase of reaction time under the test conditions [29]. H<sub>2</sub>S concentration has an immense influence on the protective ability of the sulfide film formed. As the concentration of H<sub>2</sub>S increases, the film formed is rather loose even at pH 3-5 and does not contribute to the corrosion inhibiting effect [15]. It can be speculated that the formation of the sulfide surface films has played a double role. At the low concentrations the sulfides reduced the corrosion rate most likely by coverage of the steel surface, which prevented the underlying iron from dissolving. This is supported by the facts that the sulfide films detected in the experiments were too thin to be an effective diffusion

barrier. The secondary effect, which became dominant at higher concentrations of H<sub>2</sub>S, is related to an increase of the corrosion rate. It is most likely related to the conductive sulfide films being a catalyst for the cathodic.

Figure 3 represent effect of pH and H<sub>2</sub>S concentration on corrosion rate.



**Figure 3.** Effect of pH and concentration of H<sub>2</sub>S on corrosion rate [29].

### 3 ELECTROCHEMICAL METHODES

Corrosion normally occurs at a rate determined by equilibrium between opposing electrochemical reactions. The first is the anodic reaction, in which a metal is oxidized, releasing electrons into the metal. The other is the cathodic reaction, in which a solution species (often O<sub>2</sub> or H<sup>+</sup>) is reduced, removing electrons from the metal. When these two reactions are in equilibrium, the flow of electrons from each reaction is balanced, and no net electron flow (electrical current) occurs. The two reactions can take place on one metal or on two dissimilar metals (or metal sites) that are electrically connected [30].

DC electrochemistry, and in particular, the potentiodynamic polarization scan, allows considerable information on electrode process to be acquired. Through DC polarization technique, information on the corrosion rate, pitting susceptibility, passivity as well as cathodic behavior of an electrochemical system may be obtained [31]. As the potential is increased, pitting corrosion will begin at a certain value known as the breakdown potential (EB, the lowest potential at

which pitting occurs). Since pitting corrosion relates to an increase in the oxidation rate, the EB is determined by the corresponding increase in measured current. An increase in EB is associated with higher resistance to pitting corrosion. As the potential is decreased on the reverse scan, there is a decrease in the current. However, hysteresis is observed for the reverse scan and a hysteresis loop is traced. The sample is repassivated at the potential where the reverse scan crosses the forward scan. The repassivation potential, or protection potential (EP), occurs at a lower potential than the EB. The difference between EB and EP is related to susceptibility to crevice corrosion; the greater the hysteresis in the polarization curve, the greater the crevice corrosion susceptibility.

Electrochemical corrosion experiments may also be used to determine corrosion rates (Tafel Plot), active/passive characteristics for a specific sample/solution system, passivation rates, and anodic and cathodic protection [32].



## 4 EXPERIMENTAL PROCEDURE AND SETUP

### 4.1 Research objectives

The objective of this project is to study the corrosion behavior of carbon steel in the presence of both elemental sulphur and iron sulfide in different pH level. A test temperature was selected in the range from 20°C to 80°C. The test matrix for the research is given in Table 1

**Table 1.** The Experimental test matrix

| <b>Steel type</b>    | <b>X65 (Troll tubing) polished (1000 mesh)</b>   |
|----------------------|--|
| Standard electrolyte | 0.5 M NaCl (with 0.01 M Na <sub>2</sub> S (Na <sub>2</sub> S·3H <sub>2</sub> O,) and 0.1 M HCl |
| Temperatures         | 20,40,80°C   |
| pH                   | 3,7,10   |
| Corrosion promoters  | Elemental Sulphur (S), iron(II)sulfide (FeS)-100 mesh, 99.9% metals basis                      |
| Purging              | Nitrogen (N <sub>2</sub> ) 4.0 50 liter, Yara Paraxair.  |

For the experiments carbon steel X65 is used because it is widely used material in oil and gas industry. Table 2 shows a chemical composition of carbon steel X65 (Figure 1 in appendix 1).

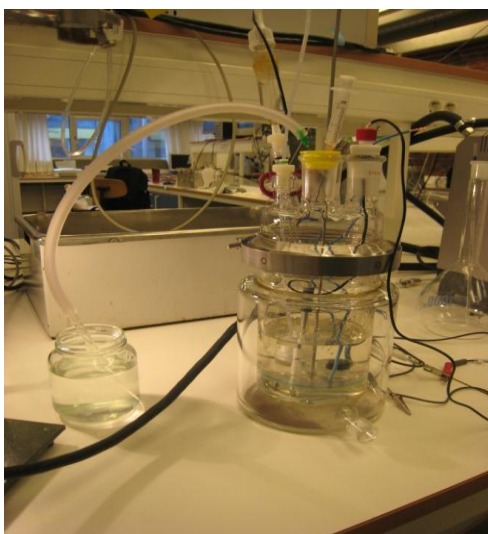
**Table 2.** Chemical composition of carbon steel X65 (from certificate)

| C:   | Si:  | Mn:  | S:    | P:    | Cr:  | Ni:  | V:    | Mo:  | Cu:  | Al:   | Sn:   | Nb:   |
|------|------|------|-------|-------|------|------|-------|------|------|-------|-------|-------|
| 0.08 | 0.25 | 1.54 | 0.001 | 0.019 | 0.04 | 0.03 | 0.045 | 0.01 | 0.02 | 0.038 | 0.001 | 0.043 |

### 4.2 Setup

The experimental setup is shown in Figure 4. The experiments were performed in a Gamry galvanic glass cell sealed with airtight glass lids designed with the ports for two working, reference, counter electrodes, port for purging tubing, port for chemical insertion and sampling. Nitrogen was bubbled for de-aeration throughout the test solution prior and during each experiment. All tubing and

wires were equipped with seals and tightened with Teflon tape so the air ingress was negligible.



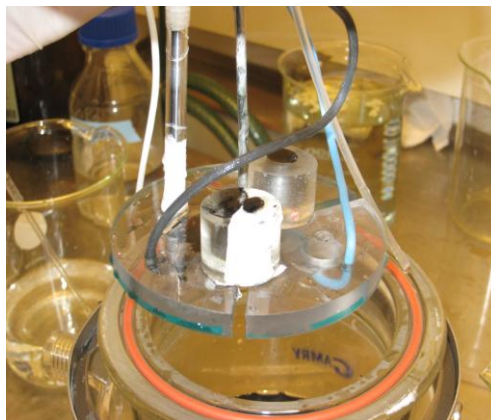
**Figure 4.** The galvanic cell.

The working electrodes were made of carbon steel X65. Coupon shape was of a cylindrical geometry, 1cm in diameter and 1 cm in height approximately with surface area approximately  $0.785 \text{ cm}^2$ . All coupons were sealed with epoxy resin such that only the end-surface area was exposed. The surfaces of all specimens were wet-polished up to 1000 grit and degreased with distilled water and ethanol, and finally dried in blowing air.

As a reference electrode a saturated calomel electrode (SCE) was used. The accuracy of the reference electrode was checked every time before and after each experiment, against a dedicated reference electrode, the difference was not more than 4-5mV in all cases. To minimize contamination of reference electrode it was mounted into narrow glass tube with the cotton plug in the end submersed into electrolyte and a thread is drawn all the way through the tube in order to prevent the formation of air bubbles and assure good electrolytic contact. All potentials were referred to the SCE. As counter electrode a platinum electrode was used (4×6×2 mm).

All chemical insertions and sampling were made by syringe molted into the air tight plug also equipped with the overpressure tube.

In order to follow the procedure the special support for two working and counter electrode was made which allowed to hold electrodes above the electrolyte surface and submersed it into the solution. This devise could keep electrodes above the electrolyte while the pH was adjusted and nitrogen was purging and be submersed easily into solution after certain time (Figure 5).



**Figure 5.** Support for two working and counter electrodes

The H<sub>2</sub>S content was made by adding sodium Na<sub>2</sub>S and HCl to the solution since Na<sub>2</sub>S turns into H<sub>2</sub>S in acidic solutions within the pH range of 1 to 5.

Gamry galvanic cell has a double-wall construction and inlet and outlet for water circulation to adjust the need temperatures.

### 4.3 Experimental procedures

All galvanic measurements were performed in 18 experiments, more than 48 hours by each. Table 3 shows the experimental overview.

**Table 3.** The experiments with the covered working electrodes

| Elemental Sulphur |             |    |    | Iron Sulfide(2) |             |     |     |
|-------------------|-------------|----|----|-----------------|-------------|-----|-----|
|                   | Temperature |    |    |                 | Temperature |     |     |
| pH                | 20          | 40 | 80 | pH              | 20          | 40  | 80  |
| 3                 | #3          | #6 | #9 | 3               | #12         | #15 | #18 |
| 7                 | #1          | #4 | #7 | 7               | #10         | #13 | #16 |
| 10                | #2          | #5 | #8 | 10              | #11         | #14 | #17 |

A procedure for measuring was made for the experiments:

- The initial open circuit potential (OCP) was measured for both working electrodes (during 90 sec);
- A cathodic potentiodynamic sweep for covered working electrode was measured at 5 to -300 mV vs  $E_{corr}$ , 0.2 mV/s, 1 meas/s after 15 minutes from beginning;
- An anodic potentiodynamic sweep for covered working electrode was measured at -5 to 150 mV vs  $E_{corr}$ , 0.2 mV/s, 1 meas/s;
- The  $R_p/E_c$  trend for covered working electrode was performed during 24 hours;
- The measurements of open circuit potential of both working electrodes were implemented after 24 hours  $R_p/E_c$  trend;
- A cathodic potentiodynamic sweep for bare working electrode was measured at 5 to -300 mV vs  $E_{corr}$ , 0.2 mV/s, 1 meas/s after 24 hours from beginning;
- An anodic potentiodynamic sweep for bare working electrode was measured at -5 to 150 mV vs  $E_{corr}$ , 0.2 mV/s, 1 meas/s after 24 hours from beginning;
- A cathodic potentiodynamic sweep for covered working electrode was measured at 5 to -300 mV vs  $E_{corr}$ , 0.2 mV/s, 1 meas/s) after 24 hours from beginning;
- An anodic potentiodynamic sweep for covered working electrode was measured at -5 to 150 mV vs  $E_{corr}$ , 0.2 mV/s, 1 meas/s after 24 hours from beginning;
- The measurements of galvanic corrosion were carried out during 24 hours.

In Series 1, one of the working electrodes was covered with elemental sulphur (S) approximately  $1.0 \text{ g/cm}^2$ . In Series 2 working electrode was covered with iron sulfide (FeS). The other electrode in both series was uncovered carbon steel. Before working electrodes were lowered to the electrolyte, purging nitrogen ( $\text{N}_2$ ) was done during at least 30 minutes.

To adjust need pH value, addition of 0.1 M  $\text{Na}_2\text{S}$  and addition of 0.5 M HCl were made through syringe.

Potentiodynamic measurements were done before 24 hours  $R_p/E_c$  trend and after.

At the end of each series galvanic corrosion measurements during 24 hours were implemented.

For galvanic measurement it was connected in zero resistance ammeter (ZRA) mode, which means one steel sample is connected as working electrode, another steel sample as the counter electrode and the reference to reference electrode.

After all experiments the working electrodes were washed with ethanol and dried in exsiccator and pictures of all were taken with light microscope for study the surface changes. Prior each next experiment cell was demounted and washed.

## 5 RESULTS AND DISCUSSIONS

All experiments could be divided in to two series with the difference in film forming agent. In Series 1 elemental sulfur was used for covering the surface of one the working electrode and in Series 2 iron sulfide was used.

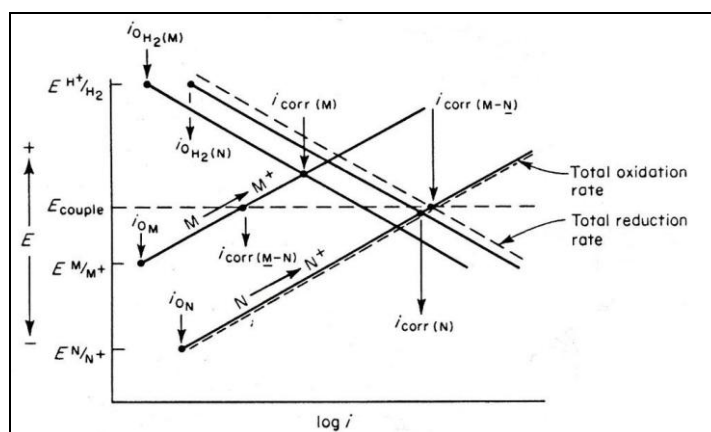
In each test OCP measurements of covered electrode were made with regard to bare working electrode at the beginning and after 24 hours of running. Table 4 includes the data of OCP in both series.

**Table 4.** Potential before and after decoupling of electrodes

|                |          | Potentials before and after decoupling of electrodes, mV |      |      |      |      |      |      |      |      |      |      |      |
|----------------|----------|--|------|------|------|------|------|------|------|------|------|------|------|
| Temperature °C | Time, hr | pH3  |      |      |      | pH7  |      |      |      | pH10 |      |      |      |
|                |          | Fe   | Fe+S | Fe   | FeS  | Fe   | Fe+S | Fe   | FeS  | Fe   | Fe+S | Fe   | FeS  |
| 20             | 0.25     | -740   | -683 | -637 | -591 | -778 | -683 | -762 | -642 | -665 | -635 | -637 | -667 |
|                | 24       | -693   | -619 | -722 | -659 | -697 | -636 | -706 | -698 | -793 | -625 | -770 | -724 |
| 40             | 0.25     | -718   | -698 | -721 | -726 | -888 | -637 | -728 | -652 | -908 | -677 | -562 | -655 |
|                | 24       | -686   | -642 | -715 | -709 | -693 | -643 | -733 | -705 | -699 | -613 | -741 | -803 |
| 80             | 0.25     | -699   | -595 | -737 | -591 | -832 | -624 | -813 | -822 | -726 | -642 | -919 | -680 |
|                | 24       | -645   | -629 | -753 | -691 | -648 | -638 | -679 | -706 | -601 | -606 | -964 | -755 |

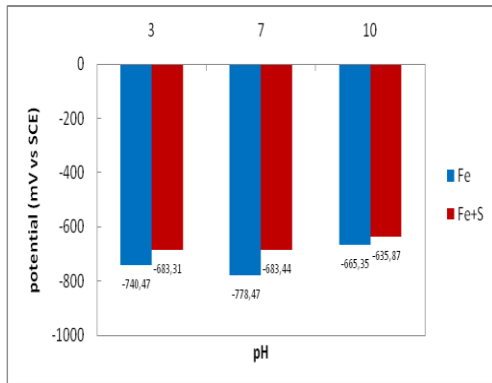
The table shows that almost in every case the OCP of bare electrode was lower than OPC of covered electrode. A higher potential of sulfur or ferrous sulfide covered electrode forces the non-covered electrode by galvanic coupling to corrode as shown in a general corrosion curve (Figure 6):

- More active metal corrodes faster when coupled, nobler metal corrodes slower;
- More active metal becomes anode, nobler becomes cathode

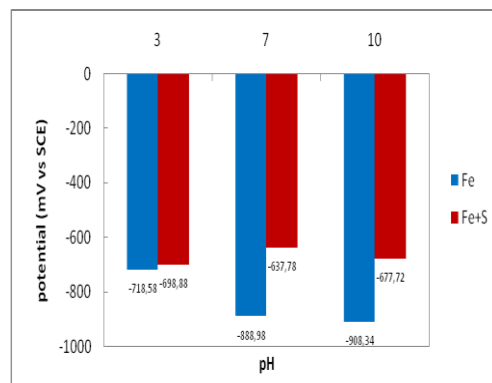


**Figure 6.** Galvanic couple between two corroding metals

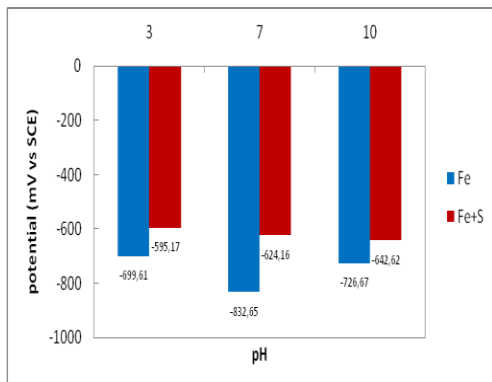
Figure 7 shows that this trend occurred in all tests in Series 1 after 15 minutes. After polarization of covered electrode and 24 hours Rp/Ec scan of coupled metals, measurements of OCP for both decoupled electrodes were repeated. Opposite behavior of the covered electrode was obtained at the pH10 at 80°C (Figure 7, f). The OCP of bare steel electrode was -606 mV (SCE) and the OCP of sulfur-covered electrode was -601 mV (SCE). This suggested that the electrode was no longer protected by a protective film. It was confirmed after the corrosion galvanic scan and pictures of surface were taken after test (Figure 20 text below). The reason of this could be the high pH and temperature conditions. Figure 8 shows the measurements of decoupled working electrodes In Series 2. At pH7 and 80°C potential was -813 for bare electrode and -822 mV (SCE) for iron sulfides-covered, at pH 10 and 40°C: -741 for bare and -803 mV (SCE) for covered electrode after 15 minutes. The covered electrode had lower potential. Same trend was obtained in measurements after 24 hours.



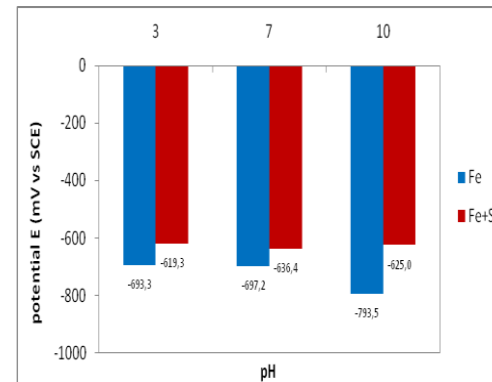
a) 20°C (Fe/Fe+S) after 15 minutes



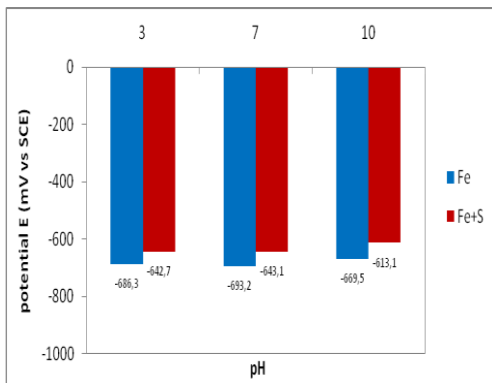
b) 40°C (Fe/Fe+S) after 15 minutes



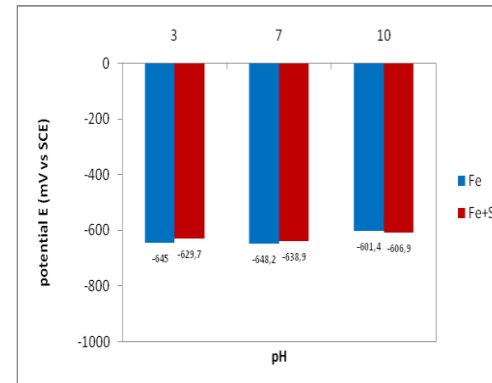
c) 80°C (Fe/Fe+S) after 15 minutes



d) 20°C (Fe/Fe+S) after 24 hours



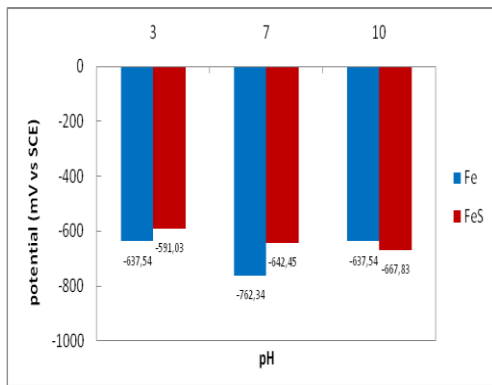
e) 40°C (Fe/Fe+S) after 24 hours



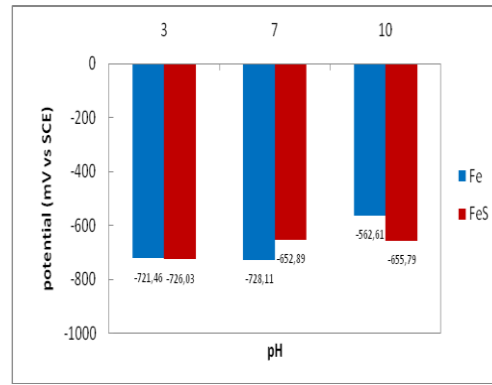
f) 80°C (Fe/Fe+S) after 24 hours

**Figure 7.** The OCP values of Fe/Fe+S galvanic couple after 15 minutes and 24 hours at different temperatures (Series 1).

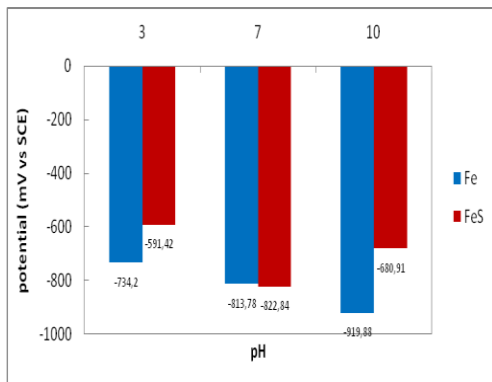




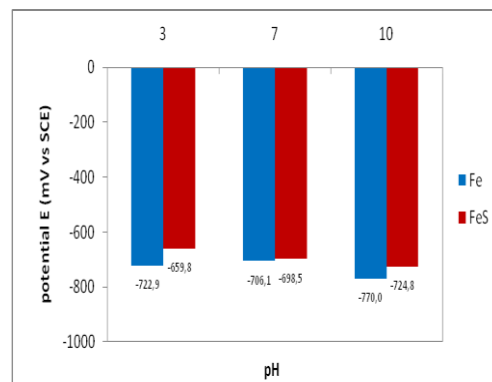
a) 20°C (Fe/FeS) after 15 minutes



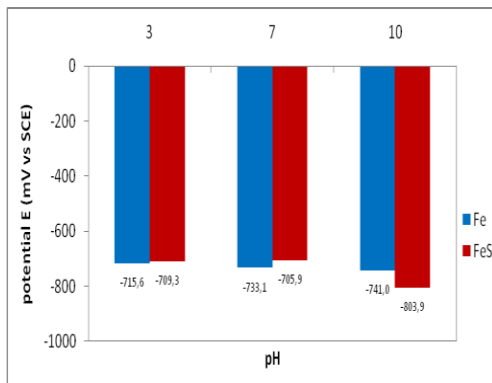
b) 40°C (Fe/FeS) after 15 minutes



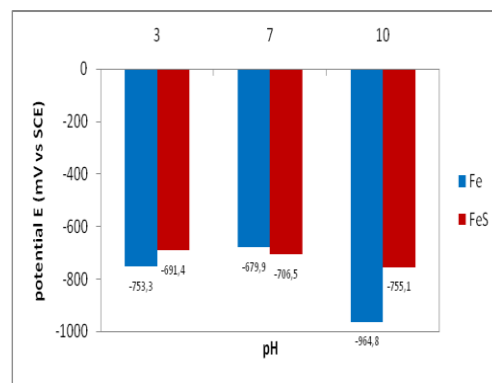
c) 80°C (Fe/FeS) after 15 minutes



d) 20°C (Fe/FeS) after 24 hours



e) 40°C (Fe/FeS) after 24 hours



f) 80°C (Fe/FeS) after 24 hours

**Figure 8.** The OCP values of Fe/FeS galvanic couple after 15 minutes and 24 hours at different temperatures.

Such a difference in OPC pointed on anodic behavior of the covered electrode though it was expected what iron sulfide would protected the surface. The films have both different structures and different electrochemical potentials, and may therefore be cathodic or anodic when they are in contact with a metal [33]. Ewing [34] has presented data showing that iron sulfide is anodic to steel at pH values above 6.5.

After 24 hours of running the OCP of covered electrode still was lower than OCP of bare one. The pictures were taken after experiments show the presence of thin black film on both electrode surfaces (Figures 26, 27 texts below; Figure 4, pictures 5, 6 in appendix), hard to remove on bare electrode and easy to peel off on covered one. After the film layer from covered with elemental sulfur was peeled off the metal remained metallic bright without detectible changes or was darkened slightly.

To see the evolution of the OCP during the test, the values of decoupled electrodes were measured in three points of time. First measurements of OPC were made after 15 minutes from the start of the tests, then after polarization of covered electrode and 24 hours of Rp/Ec trend running. Last measurements of OCP were made after polarization of both working electrodes, before galvanic corrosion measurements. The data represents in Table 5 below. The trend has been tracked between two first point regarding the time and pH.

The table shows that where were two ways of OPC evolution. Potential increases or decreases in the course of the experiment. The data tend to suggest that such decrease in potential indicates on growth of a protective film on the sample surface or if it is increase some breakage of the film or pitting occurred.

It can also be seen from the Table 5 that the potential tended to decrease with increasing in pH values in cases with elemental sulfur cover (except pH10 at 80°C) and with iron sulfide cover.

In Series 1 (Fe+S) it is difficult to observe a similar trend in changes through time. But in Series 2 (FeS) in general, OPC decreased except pH7 at 80°C and pH3 at 40°C. Also it could be noted that OCP after 15 minutes for pH7 and 80°C too low

for carbon steel. Potential has shifted from -819 to -717 mV (SCE). Comparing to working electrode covered with elemental sulfur (Series 1) at the same parameters, potential shift was -624 to -650 mV (SCE).

**Table 5.** The open circuit potential of decoupled electrodes during tests.

| Covered electrode | pH | T, °C | Time, hours |      |  |
|-------------------|----|-------|-------------|------|--|
|                   |    |       | 0.25        | 24   | Before galvanic corrosion measurements |
| Fe+S              | 3  | 20    | -683        | -619 | -607                                   |
|                   | 7  | 20    | -665        | -635 | -625                                   |
|                   | 10 | 20    | -635        | -625 | -645                                   |
|                   | 3  | 40    | -687        | -642 | -630                                   |
|                   | 7  | 40    | -637        | -643 | -652                                   |
|                   | 10 | 40    | -618        | -612 | -641                                   |
|                   | 3  | 80    | -595        | -629 | -633                                   |
|                   | 7  | 80    | -624        | -638 | -650                                   |
|                   | 10 | 80    | -639        | -609 | -612                                   |
|                   | 3  | 20    | -587        | -659 | -655                                   |
|                   | 7  | 20    | -640        | -698 | -723                                   |
|                   | 10 | 20    | -667        | -724 | -786                                   |
| FeS               | 3  | 40    | -724        | -709 | -789                                   |
|                   | 7  | 40    | -650        | -705 | -732                                   |
|                   | 10 | 40    | -654        | -803 | -839                                   |
|                   | 3  | 80    | -575        | -691 | -716                                   |
|                   | 7  | 80    | -819        | -706 | -717                                   |
|                   | 10 | 80    | -675        | -754 | -808                                   |

Thermodynamically, according to the Nernst equation, as the pH and temperature of the electrolyte increases the electrode potential of a metal decreases [35].

### **Series 1**

Further the data will be representing divided in two series. Some of the diagrams were plot in Gamry Echem Analyst program, which make the work with numerous values easier.

To investigate the cathodic and anodic behavior potentiodynamic measurements for the covered electrode were carried out after 15 minutes from beginning of each test and one more time after 24 hours Rp/Ec trend for both of working electrodes.

Figures 9-11 show the potentiodynamic polarization curves of X65 carbon steel at various pH levels and different temperatures in Series 1.

The Ecorr potential was not the same after a cathodic sweep and therefore many of the curves showed not an overlap of starting potential (Ecorr) for the anodic sweep.

Pauses in 15 minutes between cathodic and anodic measurements were made, but still some curves deviated in the starting potential. As polarization was start with the cathodic current steps, it was suggested that the mixed potential at the beginning of cathodic step curve.

The effect of the corrosion products is that the galvanic current be reduced by the increase in the ohmic resistance and the change of the corrosion potential to more noble values [36]. It was expected that such changes would be occurred with decreasing in the pH level and temperature which may cause to dissolution of protective layer.

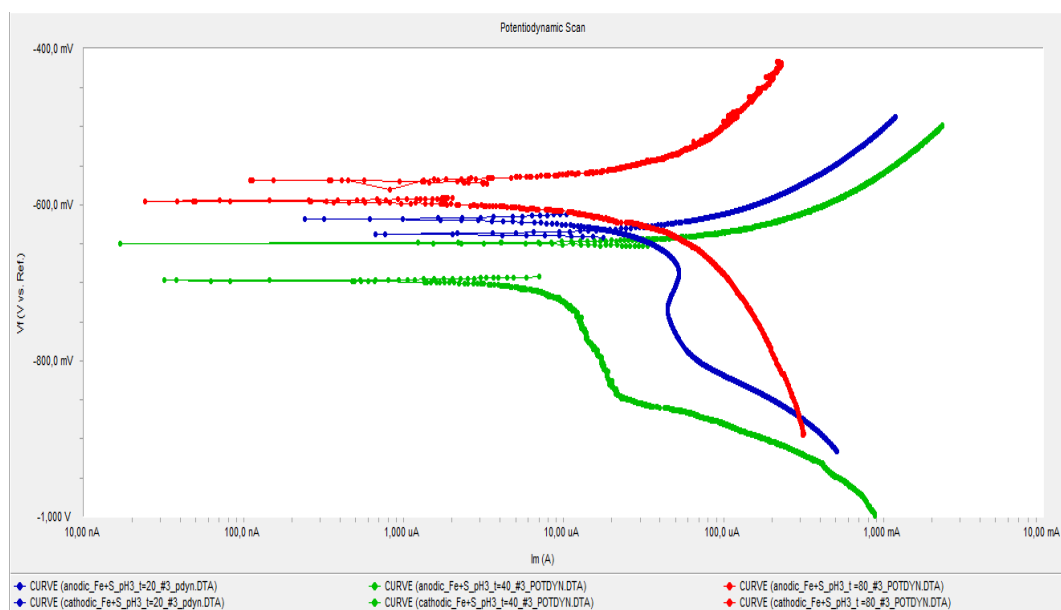
Figures 9-11 show stable behavior of anodic curves with increasing in pH. The anodic current increased with increasing in pH. This could be due to the fact that corrosion process involved formation and dissolution of corrosion products, always maintaining the surface active [37]. Shift in potentials was in a range of

-568 to -609 mV (SCE). Nobler potential was observed at pH3 at 80°C. More negative potential was at pH3 at 40°C (Figure 9).

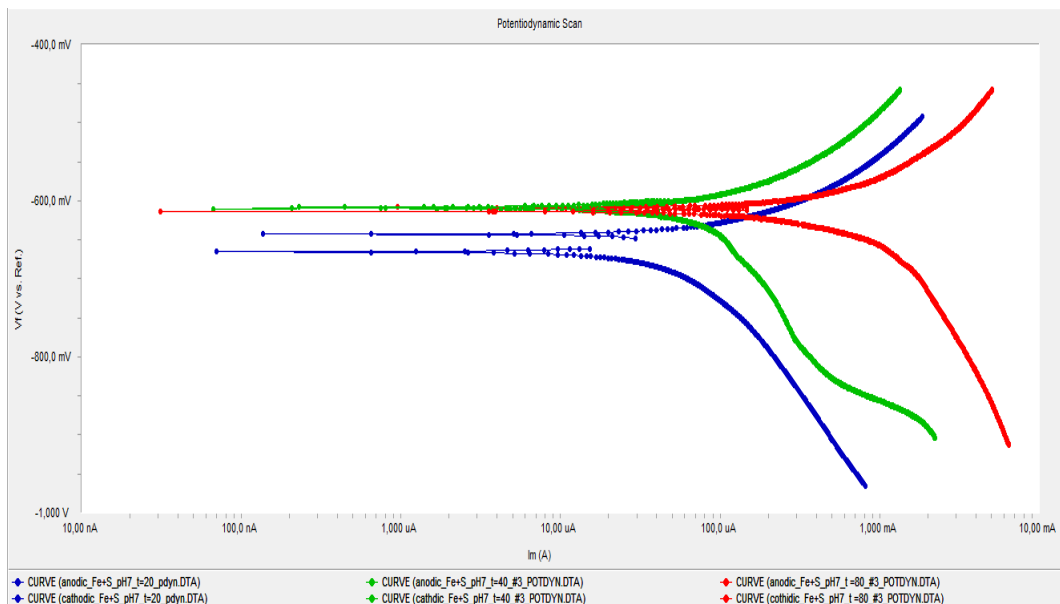
Figure 9 clearly showed hydrogen reduction region and reduction of water or sulfur species in environment due to a more catalytic film under the conditions of 20, 40°C at low potential. Same behavior of cathodic reaction could be seen at pH7 at 40°C (Figure 10). At this pH level the more negative potential -665 mV (SCE) was observed at 20°C.

The higher current was observed at pH7 at 80°C (Figure 8). This allowed expecting higher corrosion rate under these conditions. That was confirmed during the Rp/EC trend measurements (Figure 10).

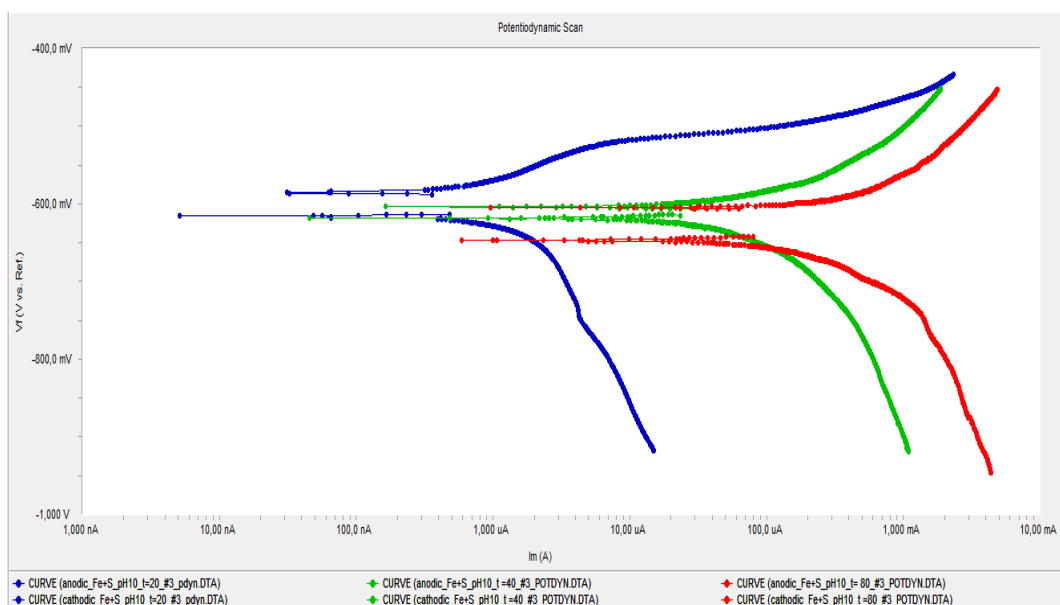
Figure 9 shows that at pH7 at 20°C, the anodic current increased significant in the region with a small shift in potential. Then potential rose slowly to -433 mV with high applied current.



**Figure 9.** Potentiodynamic sweeps for covered with elemental sulfur working electrode at pH3 at 20°C (blue), 40°C (green), 80°C (red) after 15 minutes.

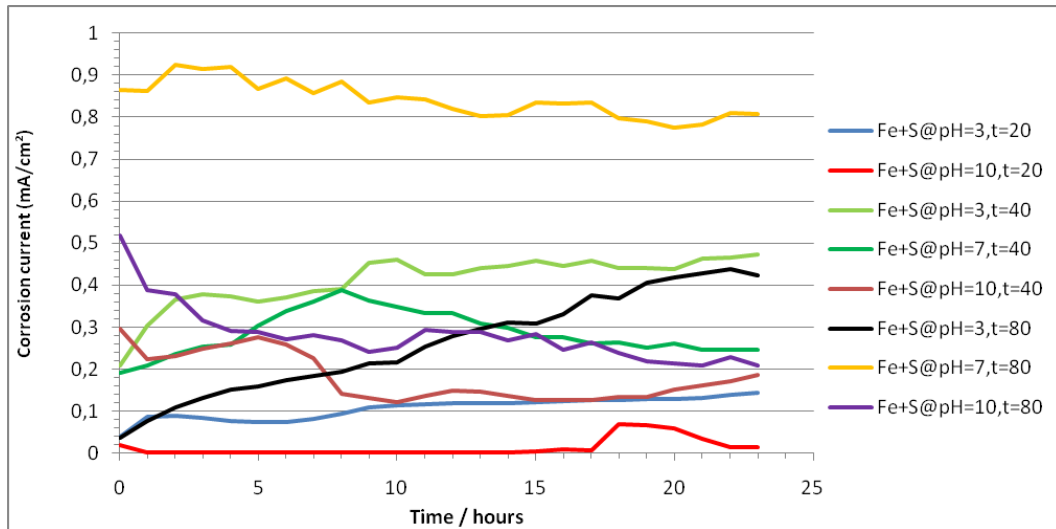


**Figure 10.** Potentiodynamic sweeps for covered with elemental sulfur working electrode at pH7 at 20°C (blue), 40°C (green),80°(red) after 15 minutes.



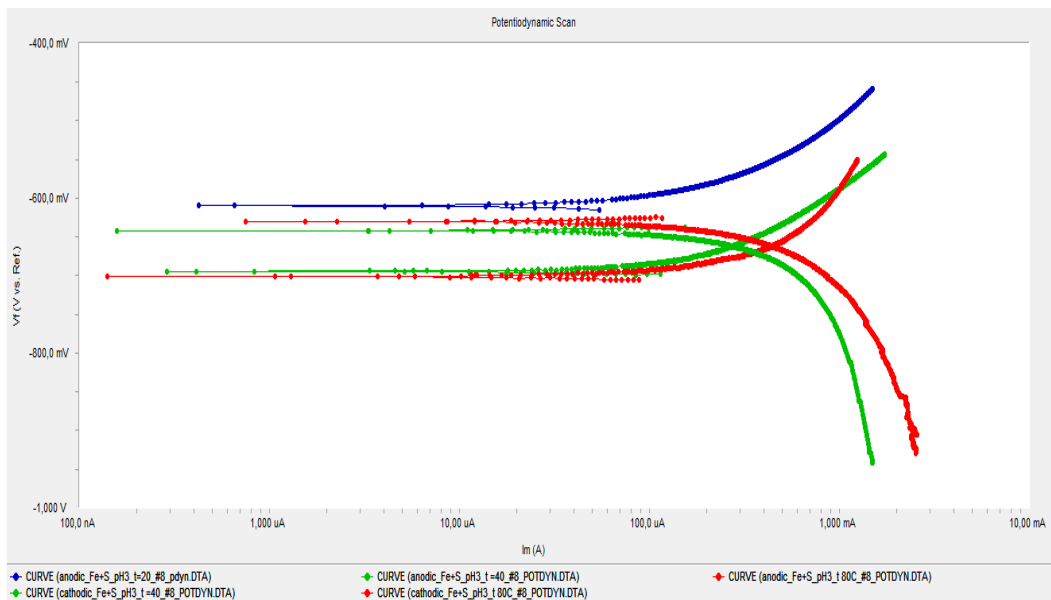
**Figure 11.** Potentiodynamic sweeps for covered with elemental sulfur working electrode at pH10 at 20°C (blue), 40°C (green),80°(red) after 15 minutes.

After potentiodynamic polarization tests,  $R_p/E_c$  trend measurements were made to determine the corrosion current density. Figure 12 diagrams the corrosion current density in all tests in Series 1.

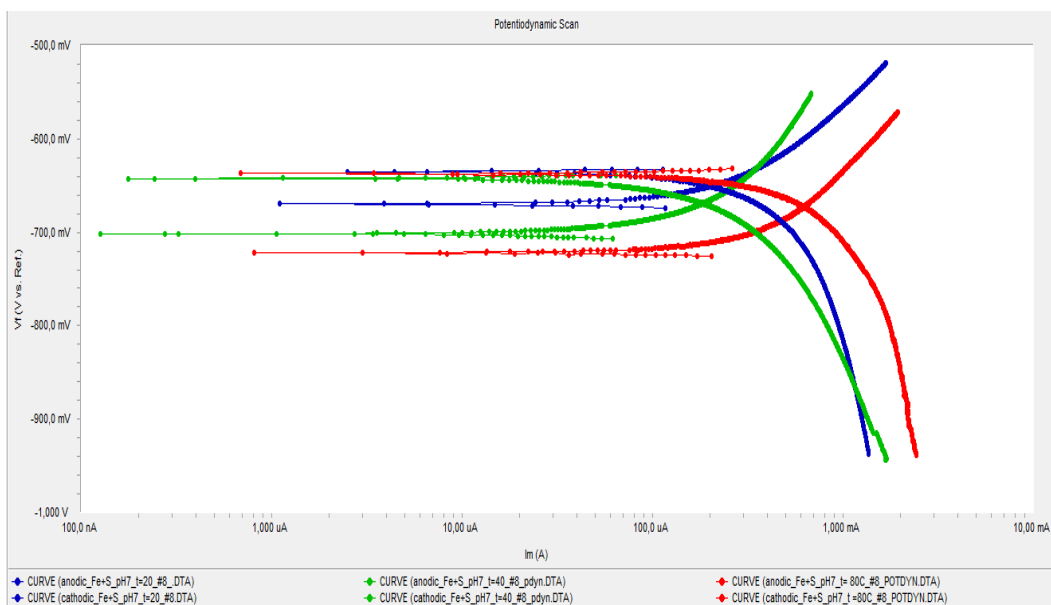


**Figure 12.** Changes in corrosion current density in time for decoupled sulfur-covered electrode.

As can be seen from the Figure 12, the higher current density was at pH7 at 80°C. This is surprising high value compared to the other tests results. It was expected to see the higher values of current density at pH3. One possible reason for large divergence in the results could be the specimens were prone to edge attack. Also it could be due to difficulties in adjustment of pH level. In general highest values are observed at pH3 at 40, 80°C. These two lines have tend continuously increase in current density over a period of experiment. In other hand the lines at pH10 at 40, 80°C tended to stabilize and decrease with time. At the pH10 at 20°C current density was almost zero during 17 hours of running and increased not significant after. It means that the covered electrode corroded less because it had the lowest current density. After 24 hours of  $R_p/E_c$  measurements polarization scans were taken. Figures 13-15 show the potentiodynamic curves for covered with elemental sulfur electrode after 24 hours  $R_p/E_c$  trend.

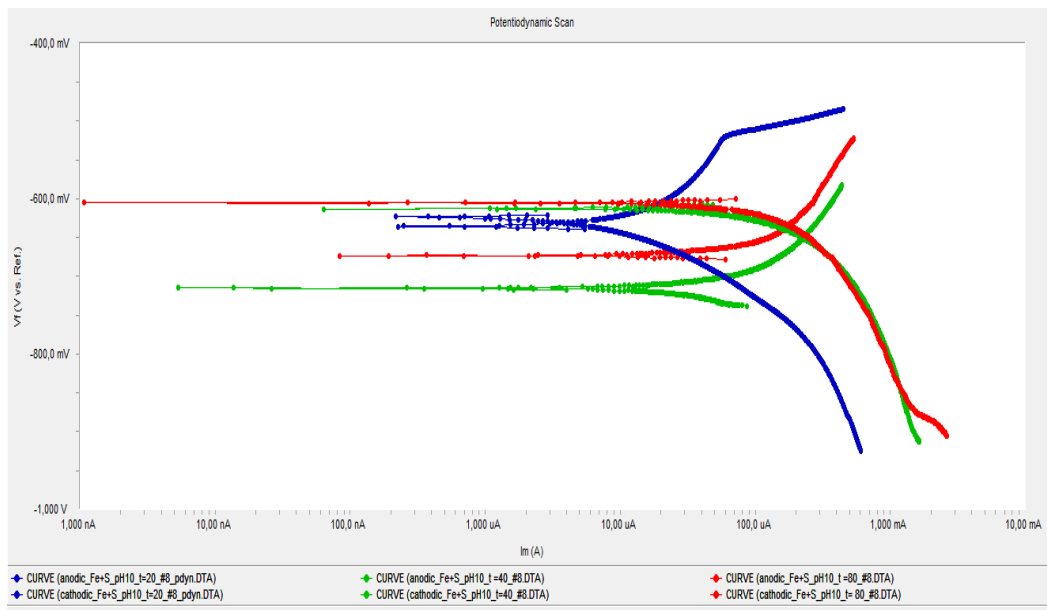


**Figure 13.** Potentiodynamic sweeps for covered with elemental sulfur working electrode at pH3 at 20°C (blue), 40°C (green),80°(red) after 24 hours.



**Figure 14.** Potentiodynamic sweeps for covered with elemental sulfur working electrode at pH7 at 20°C (blue), 40°C (green),80°(red) after 24 hours.





**Figure 15.** Potentiodynamic sweeps for covered with elemental sulfur working electrode at pH10 at 20°C (blue), 40°C (green), 80°C (red) after 24 hours.

In all cases, the steel showed only an active behavior, anodic dissolution, without evidence of any passive layer, except pH10 at 20°C (Figure 15). Under these parameters, potential stopped to increase rapidly with not significant increasing in current at -523 mV (SCE). Then current was increased without big increasing in potential. The cathodic potential decreased comparing to pH7. It may be suggested as inhibition effect due to formation of corrosion products on surface.

The shape of the rest curves practically remained the same with the pH changes. The potential values lies between -609 and -701 mV (SCE). The lower anodic potential under the conditions of pH7 at 80°C with higher current and corrosion rate (Figure 12). The anodic curves obtained show very similar current, regarding to pH changes.

Along with the polarization studies of covered electrode the potentiodynamic sweeps of bare steel electrode were carried out. Table 6 shows the  $E_{corr}$  potentials for bare and for covered decoupled electrodes during further polarization measurements.

**Table 6.** Comparison of E<sub>corr</sub> potential for decoupled electrodes.

| pH | Temperature, °C | E <sub>corr</sub> after 15 minutes (Fe+S), mV | E <sub>corr</sub> after 24 hours (Fe+S), mV | E <sub>corr</sub> after 24 hours (Fe), mV |
|----|-----------------|---|---|---|
| 3  | 20              | -618  | -609  | -691                                      |
|    | 40              | -697  | -642  | -685                                      |
|    | 80              | -595  | -629  | -648                                      |
| 7  | 20              | -665  | -635  | -809                                      |
|    | 40              | -608  | -642  | -893                                      |
|    | 80              | -613  | -613  | -647                                      |
| 10 | 20              | -615  | -623  | -769                                      |
|    | 40              | -618  | -613  | -690                                      |
|    | 80              | -646  | -604  | -634                                      |

From Table 6 it can be seen that values of E<sub>corr</sub> potential for bare carbon steel electrode after 24 were lower than potential of covered electrode.

Figures 16-18 represent the obtained polarizations curves for bare electrode. It can be seen, that where is no such big difference in anodic and cathodic potentials which was in the tests with covered electrode. The potential region was obtained between – 647 and -926 mV (SCE) and decreased with increasing in pH. The more negative potential was under conditions of pH10 at 20°C (Figure 18). This is permit to suggest a higher corrosion rate at bare steel. From Figure 10 it can be seen that the covered electrode in the galvanic couple under same conditions showed a lower current density and corrosion rate.

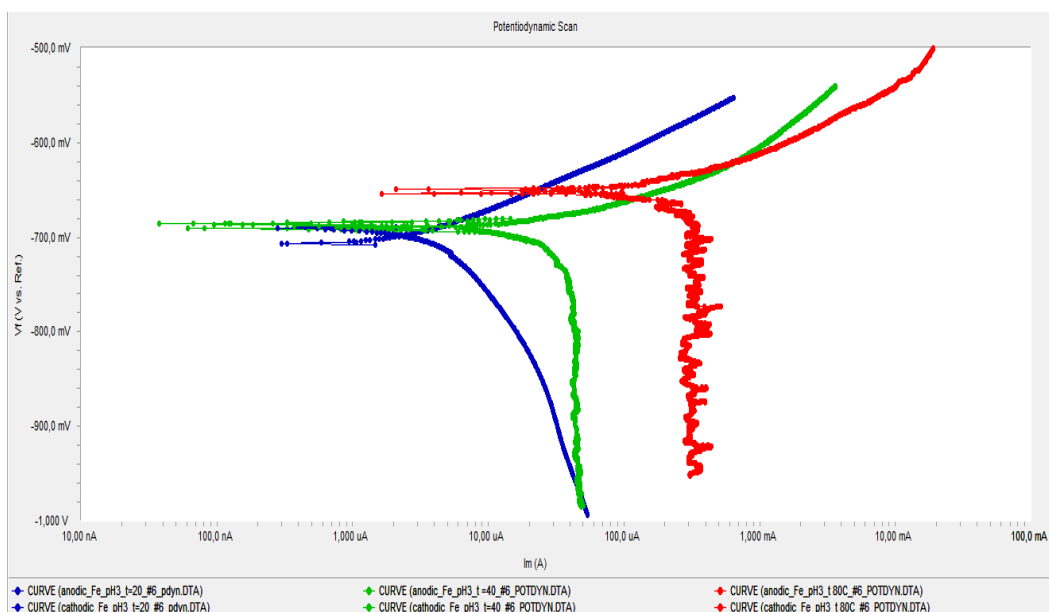
Under the conditions of pH3 at 40, 80°C it can be seen a decrease in cathodic reactions.

It has been found that potential-based current oscillations occurred during the tests of bare steel electrode. During the scans at pH10 the data of anodic and cathodic steps at 80°C have been lost (Figure 18). At these conditions the more sensitive oscillations were obtained. There are several possible reasons for such behavior [38]:

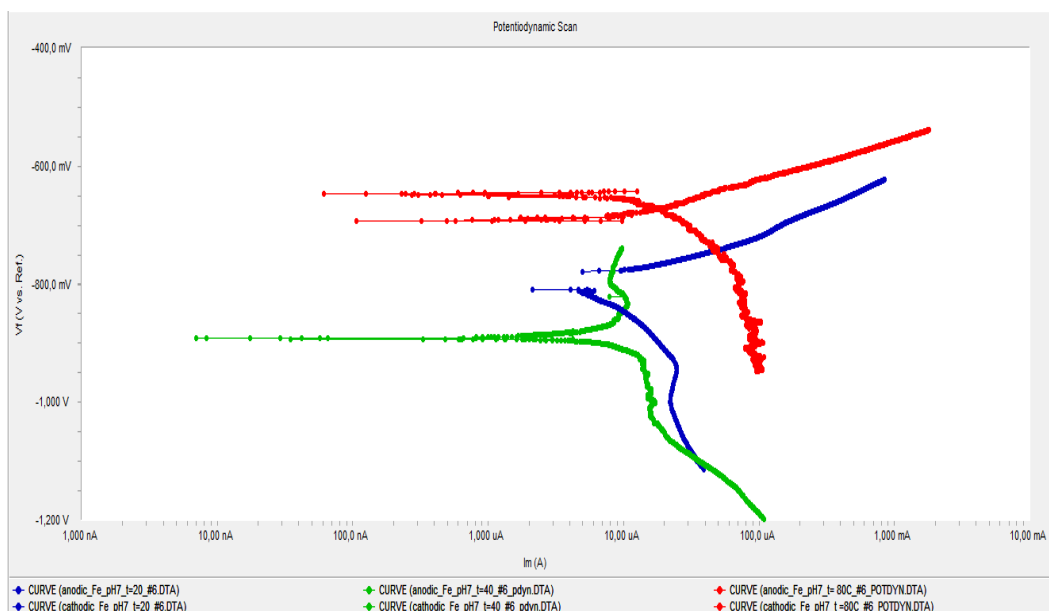
- The instrument
- The cell/electrodes
- The chemistry

- The local electronic environment

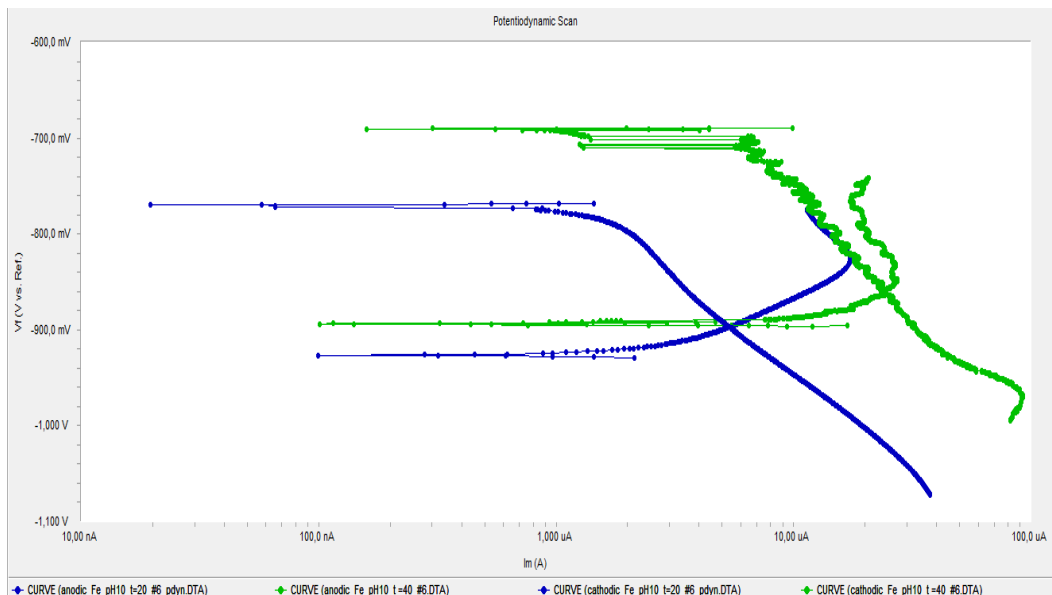
The possible reason of such oscillation should be investigated further.



**Figure 16.** Potentiodynamic sweeps for bare working electrode at pH3 at 20°C (blue), 40°C (green), 80° (red) after 24 hours.



**Figure 17.** Potentiodynamic sweeps for bare working electrode at pH7 at 20°C (blue), 40°C (green), 80° (red) after 24 hours.



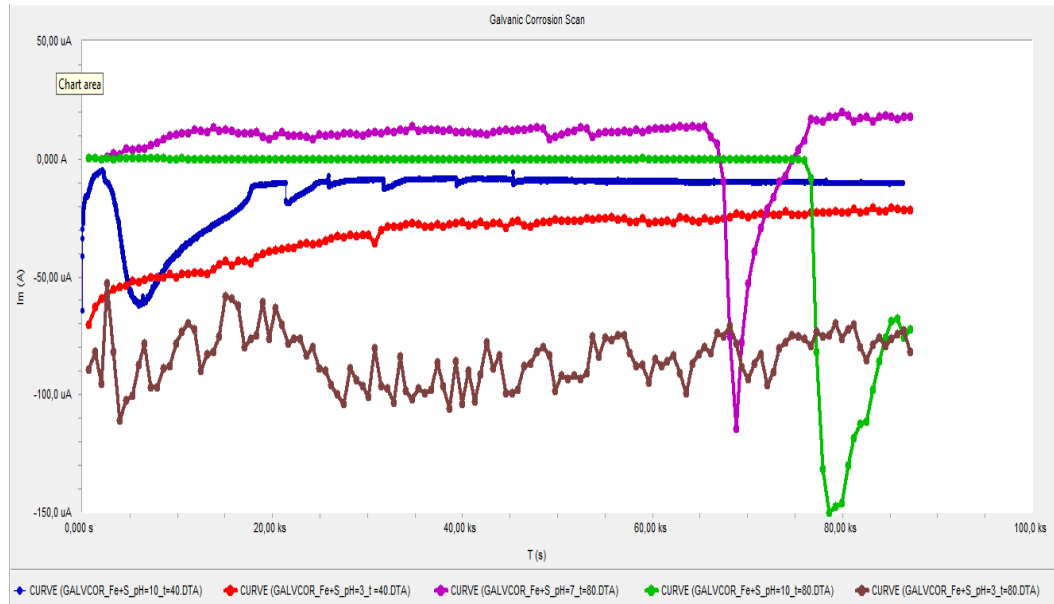
**Figure 18.** Potentiodynamic sweeps for bare working electrode at pH10 at 20°C (blue), 40°C (green), after 24 hours.

It can be seen from Figures 16-18 that the potentials in these tests were very low and decreased with increasing in pH. The potential also shifted slight with increasing of the temperature in noble direction. In the test under condition of pH10 at 80°C the potentiostat could not record the cathodic and anodic curves for the unknown reason (Figure 18).

Figure 19 show the galvanic corrosion measurements after polarization of the both electrodes. Due to a set-up error at the start of this work, the curves for first four experiments (at pH7 at 20, 40°C and at pH10 at 20, 40°C). Rest curves showed that the corrosion rate increased with the temperature increasing. Lei Zhang et al reported that within the temperature increasing to 90°, the corrosion type of X65 steel changes from general corrosion to localized corrosion [40]. The Figure 20 shows the temperature effect on corrosion rate of steel.

More stable and more negative current value covered coupon showed at pH3 at 80°C. At pH7 at 80°C, Fe+S electrode showed positive current value first eighteen hours. Then current very rapidly decreased from 13.7  $\mu\text{A}$  to -114.5  $\mu\text{A}$  pointed out pitting. Presence of pitting was observed after the pictures of surface were

tacken (Figure 1, picture 4 in appendix 2). During next hour it increased to 16.83  $\mu\text{A}$ . At pH10 at 80°C current was near zero value first 21 hours. During one hour it dropped till -150.5  $\mu\text{A}$  rapidly. This permit to suggest the pitting on the surface of covered electrode. Next two hours current rose.

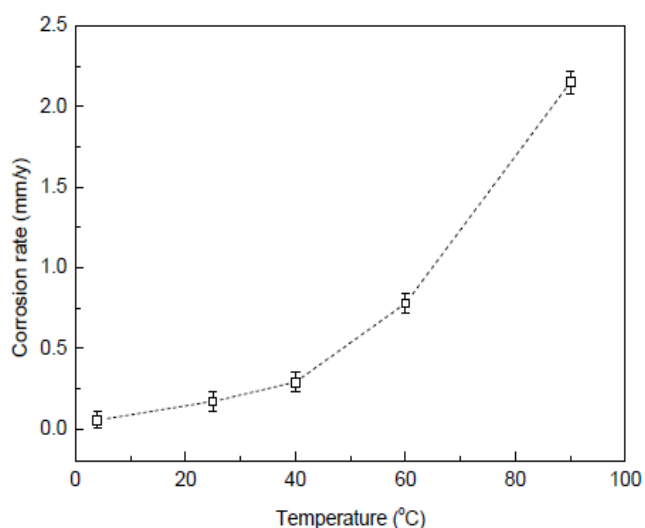


**Figure 19.** Galvanic corrosion: pH10 at 40°C (blue); pH3 at 40°C (red); pH7 at 80°C (purple); pH10 at 80°C (green); pH3 at 80°C (brown).

**Table 7.** Galvanic current for covered electrode in coupling Fe/Fe+S ( $\mu\text{A}$ ).

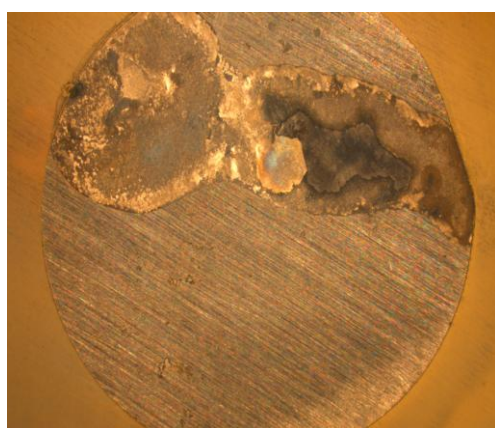
| temperature | pH3    | pH7   | pH10   |
|-------------|--------|-------|--------|
| 20          | -----  | ----- | -----  |
| 40          | -21.47 | ----- | -10.15 |
| 80          | -81.73 | 17.75 | -0.819 |

Table 7 shows the data from galvanic scan in Series 1. Only under conditions of pH7 at 80°C current showed positive value. Lack of the values in rest experiments not allowed tracing the trend under conditions of 20°C. The reason of failure could be investigated in future work.



**Figure 20.** Effect of temperature on corrosion rate of the steel [40].

Figure 21 shows the picture of the bare working electrode taken after the end of the experiment at pH10 at 80°C. It shows that steel suffered from general corrosion. Figure 22 is the picture of the covered with elemental sulfur working electrode in the same experiment. It can be seen that the surface is covered with a thick black film which has protected surface from general corrosion, but presence of pitting was also observed.



**Figure 21.** Surface of bare carbon steel electrode (pH10 at 80°C).



**Figure 22.** Surface of covered with elemental sulfur carbon steel electrode (pH10 at 80°C).

Before the exposure in electrolyte, the surface of one working electrode which suggested being covered was coated with powder (elemental sulfur or iron sulfide). To hold the powder the Teflon tape was used. Not the entire surface was covered with film agent. This is easier to see in Figure 23.

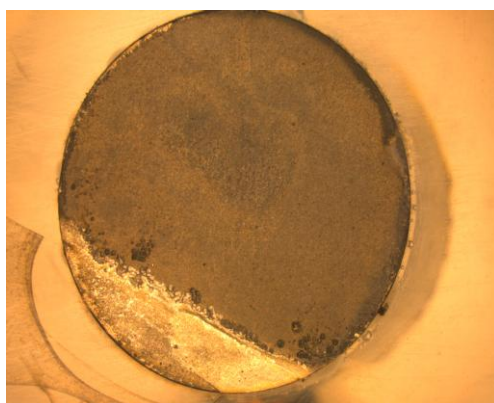


**Figure 23.** Picture of covered with Teflon tape and bare working electrodes.

Figure 24 shows one of the example of this situation there the uncovered region suffered from localized/pitting corrosion in the border of tape and thick black

film under the tape. Elemental sulfur particles can form a block area on coupon when coupons are partially covered by elemental sulfur which increases the tendency of localized corrosion. Meanwhile, sulfur particles can absorb sulfur ions to form  $S_{y-1} \cdot S^{2-}$  which can directly participate in cathodic reactions. When coupons are uniformly covered by elemental sulfur particles in forms of deposited, molten or paste characters, corrosion occurs just under the sulfur-coverage area [39].

Moreover, during the all tests formation of thin black layer was observed on the surface of the bare carbon steel electrode. Could be likely because of both electrodes were in the same cell and precipitation of dissolved sulfur occurred.



**Figure 24.** Surface of covered with elemental sulfur electrode (pH10 at 20°C) after removal of Teflon tape.

## Series 2

Experimental procedure for Series 2 was the same as for Series 1. One of the working electrodes in couple was covered with iron sulfide powder instead of elemental sulfur. During the tests bare electrodes behaved usually like an anodes (see the Table 5). In three tests of nine the opposite results were observed. The covered electrode was a cathode. But only at conditions of pH10 at 40°C covered electrode reminded cathode till the end of running. Rest potentials decreased with the time.

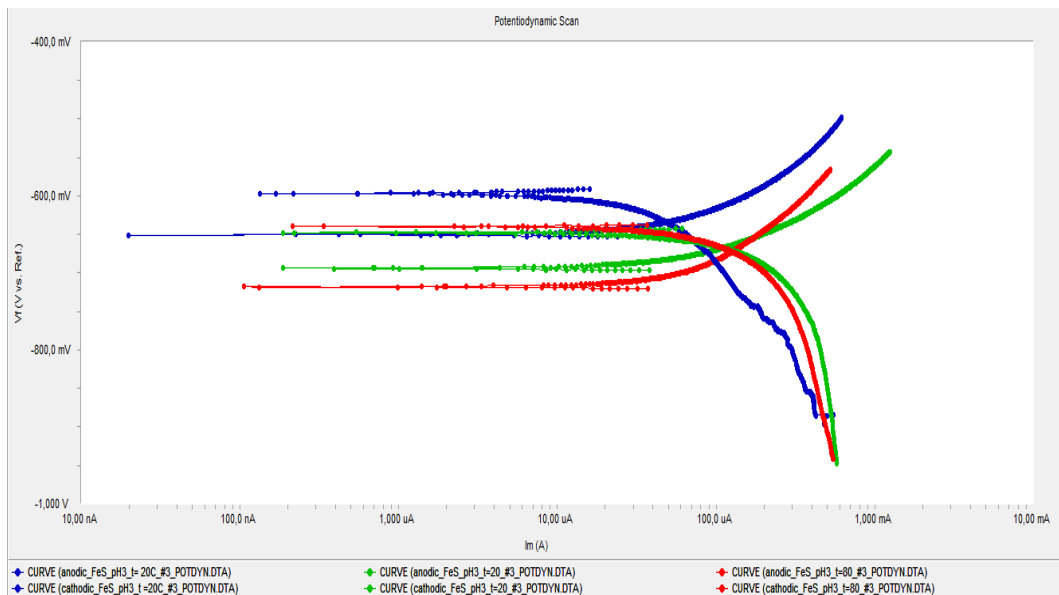


Figures 25-27 show the polarization scan for FeS electrode at pH 7-10 at the different temperatures after first 15 minutes of experiments. With increasing in pH the potential decreased not significantly. Corrosion rate increased with increase of the temperature. The shift of the potential lies in a region between -579 and -847 mV (SCE). From Figures 25 and 27 it can be seen the suppressed the cathodic reactions in the lower overpotential ranges.

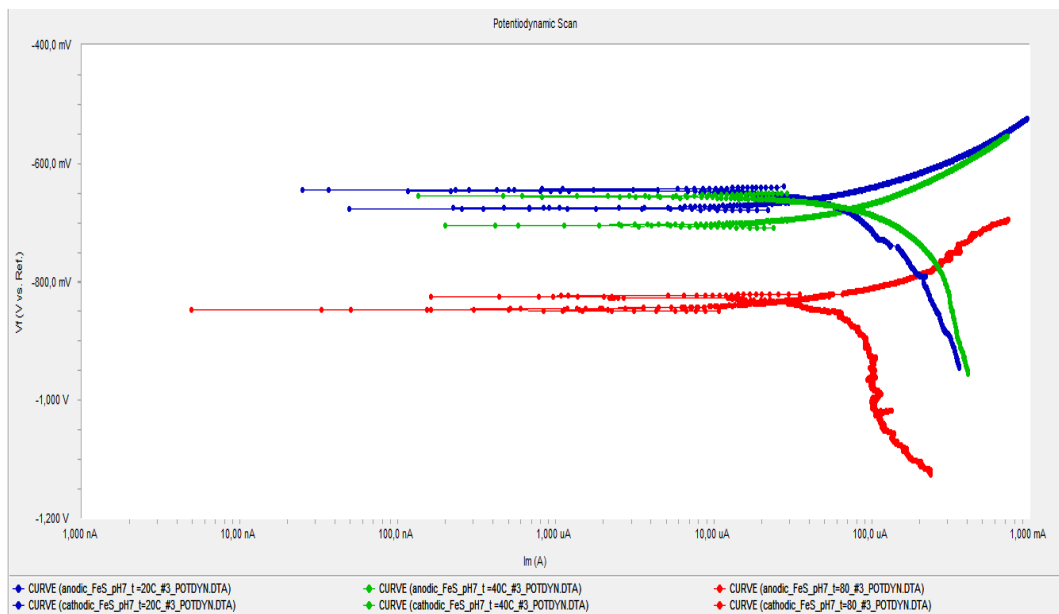
At pH3 at 20°C on cathodic curve can be seen small oscillation with increasing in current, whereas the anodic current was not affected (Figure 25).

In Figure 24 it can be seen that the polarization curves (pH7 at 80°C) a lower starting potential for the cathodic and anodic sweeps. The anodic potential was -847 mV (SCE). The cathodic line represents the hydrogen reduction region and slight shift in current for further cathodic reaction, whereas the anodic current was affected and increased with increasing in potential. The presence of oscillation was observed in both cathodic and anodic sweeps. One of the reasons could be that the potentials of the reactions were in very negative region (up to -1.125 V for anodic steps).

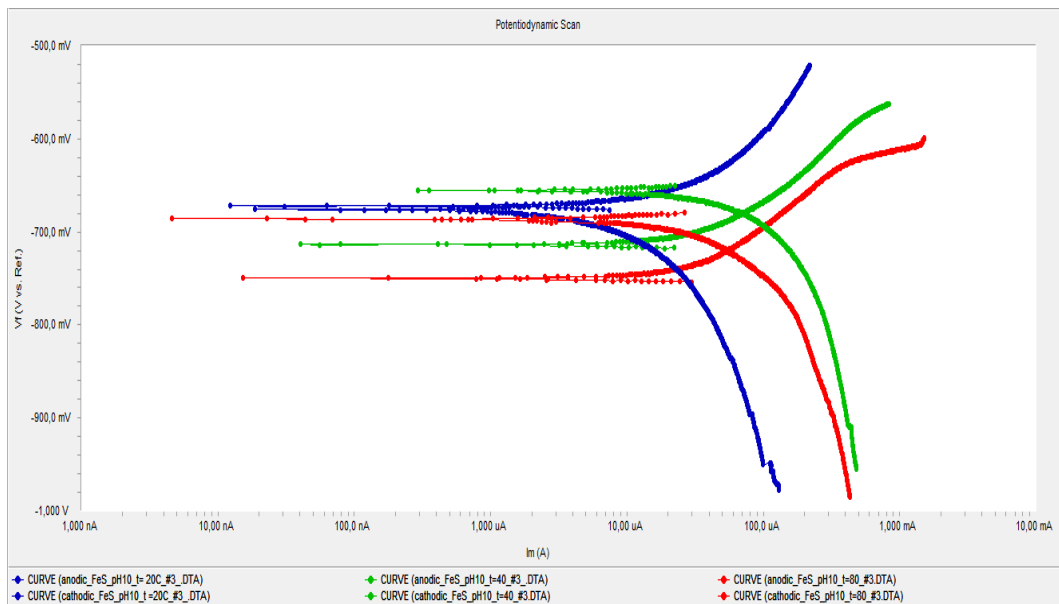
At pH10 at 80°C it can be seen that the limiting current which affected anodic reactions after the potential increased to approximately -625 mV (SCE) (Figure 27). The passivation region was obtained. All curves (Figures 25-27) show no significant shift with the temperature and pH changes (only pH7 at 80°C). The potential decreased slightly with the temperature and pH increasing. More negative values obtained at pH7.



**Figure 25.** Potentiodynamic sweeps for covered with iron sulfide working electrode at pH3 at 20°C (blue), 40°C (green),80°(red) after 15 minutes.

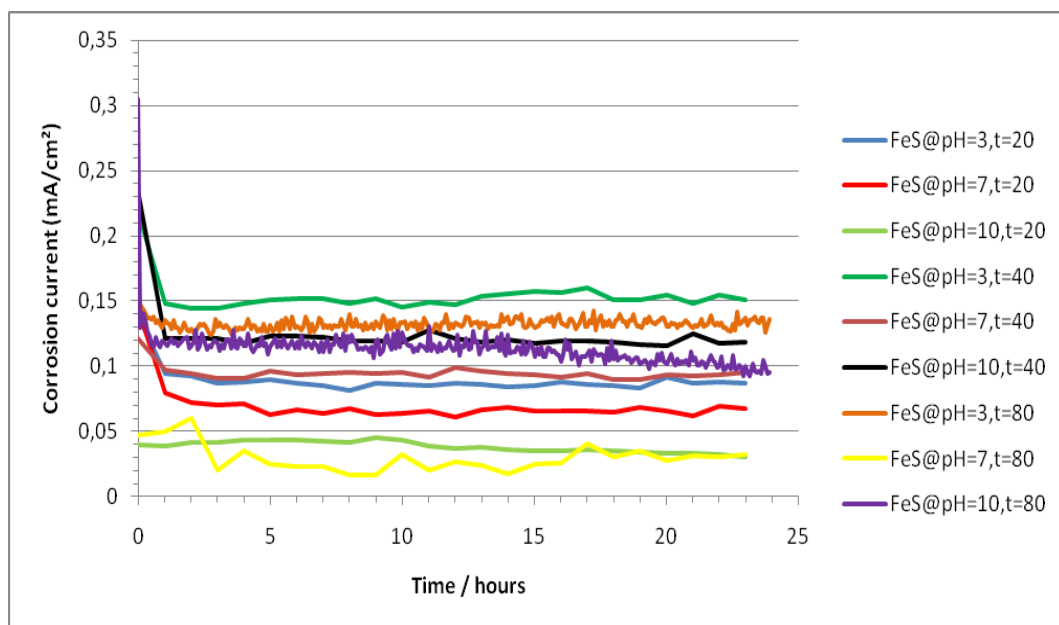


**Figure 26.** Potentiodynamic sweeps for covered with iron sulfide working electrode at pH7 at 20°C (blue), 40°C (green),80°(red) after 15 minutes.



**Figure 27.** Potentiodynamic sweeps for covered with iron sulfide working electrode at pH10 at 20°C (blue), 40°C (green),80°(red) after 15 minutes.

The galvanic corrosion measurements have been performed during 24 hours Rp/Ec. Figure 28 shows the results.



**Figure 28.** Changes in corrosion current density in time for decoupled iron sulfide- covered electrode.

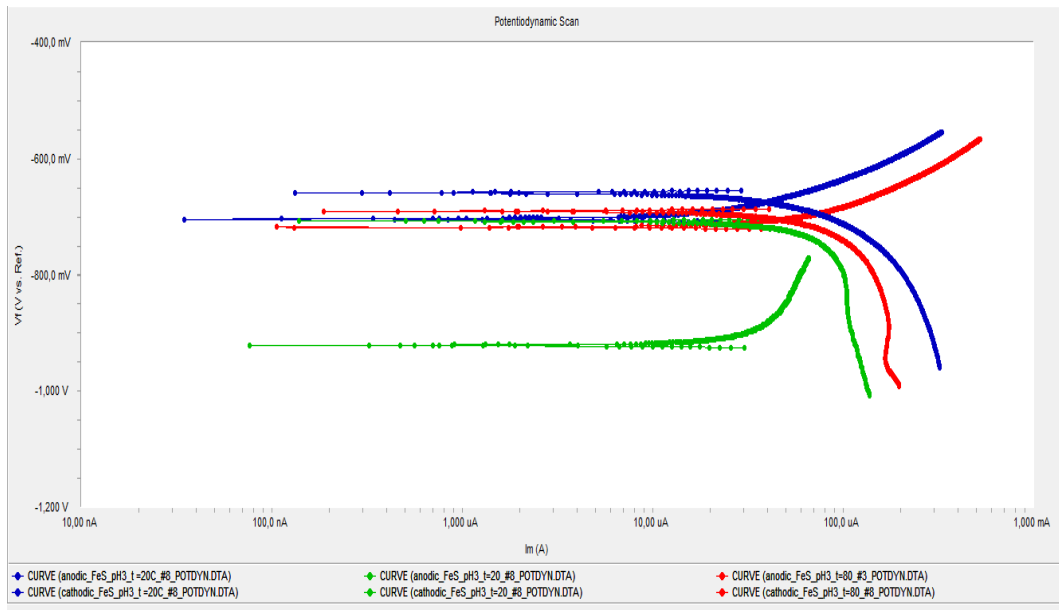
At the beginning of all measurements current densities had maximum values but during first hours were decreased and stabilized (Figure 28). The higher value at the start shows line pH10 at 80°C. The line pH10 at 20°C shows most stable trend.

The higher final value of current density is at pH3 at 40°C. As expected the higher rate was at low pH value (pH3) and high temperatures (40, 80°C). The theory considers the iron sulfide produced by corrosion is insoluble at normal pH's and can form the film which protects metal. Lower pH makes iron sulfide more soluble, thus keeping the film from formation.

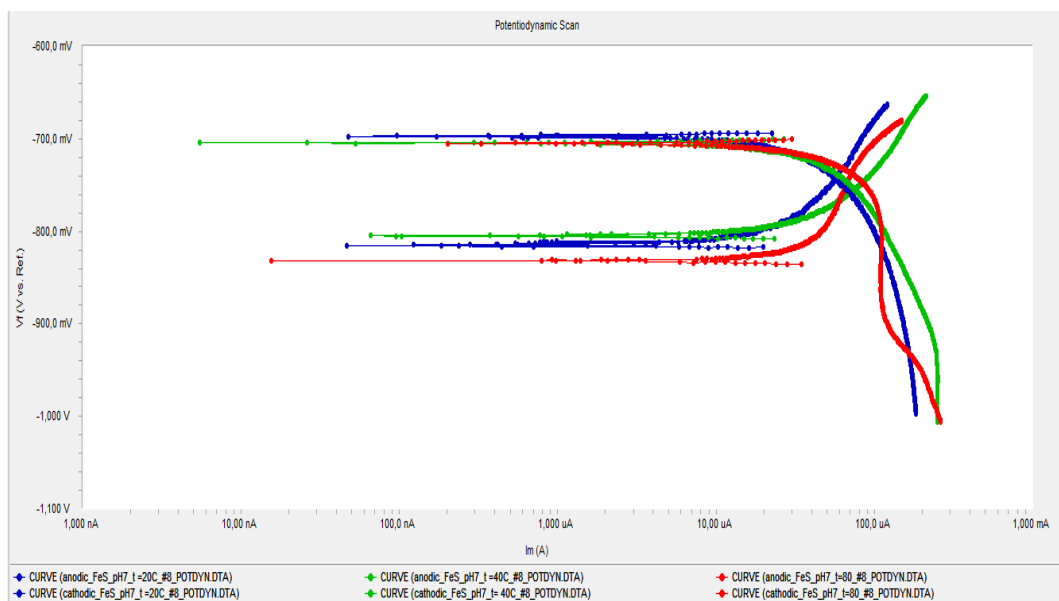
But also the relative high values were at pH10 at 40, 80°C, which does not match the theory.

As in Series 1, after Rp/Ec trend the polarizations scans were made. The big difference between anodic and cathodic potential values was observed. The shift in potentials lies in the range between -658 and -952 mV (SCE). The potential decreased with pH increasing. At pH3 at 40°C anodic potential showed the lower value (-920 mV (SCE)) at 40°C (Figure 29).

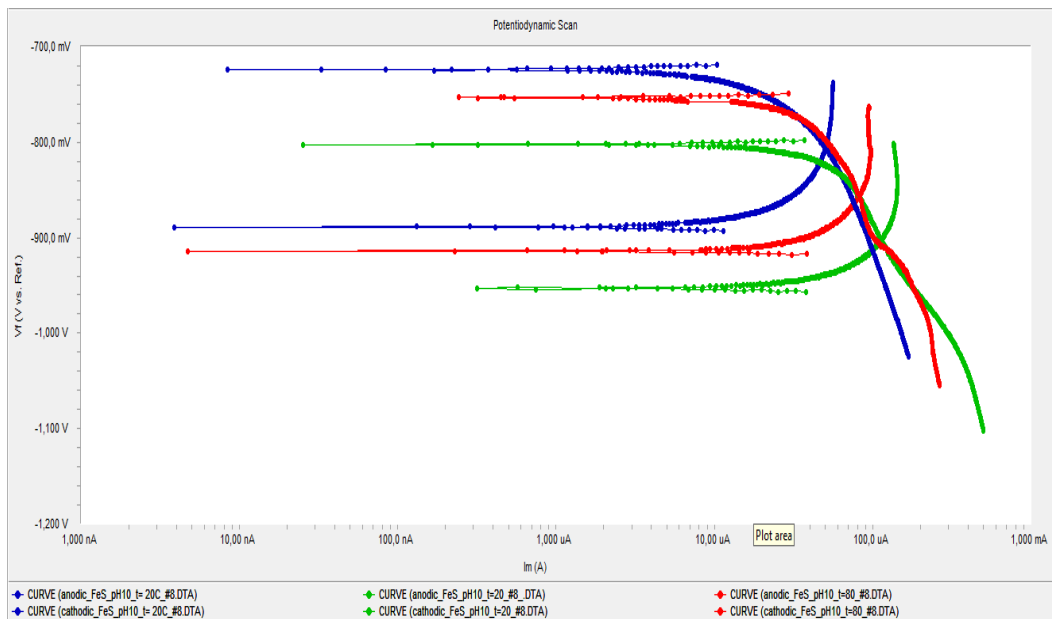
During the tests at pH 7, the rapid increase in applied potential of both anodic and cathodic reaction was observed with sufficiently negative values (Figure 30). Current increased not significantly. At the temperature 80°C, cathodic line shows some reduction of non hydrogen species, suggesting reduction of water and sulfur species. Figure 31 shows very low potential values for the both anodic and cathodic steps. It also can be observed in Table 5. The suddenly increase of anodic potentials with no increasing in current permit to suggesting a passive region. The cathodic reactions were dominated. That could be interpreted as a protective film formation. This was confirmed by visual inspection of the coupon after removal from the cell. Only the surface of the coupon exposed at pH10 at 80°C had an evidence of the localized corrosion (Figure 2, picture 2 in appendix 2). The rest two coupons were covered with thin black film non-adherent and cracks easily. The surface remained metal bright (Figure 2, picture 6 in appendix 2) after the film was removed.



**Figure 29.** Potentiodynamic sweeps for covered with elemental sulfur working electrode at pH3 at 20°C (blue), 40°C (green), 80°C (red) after 24 hours.

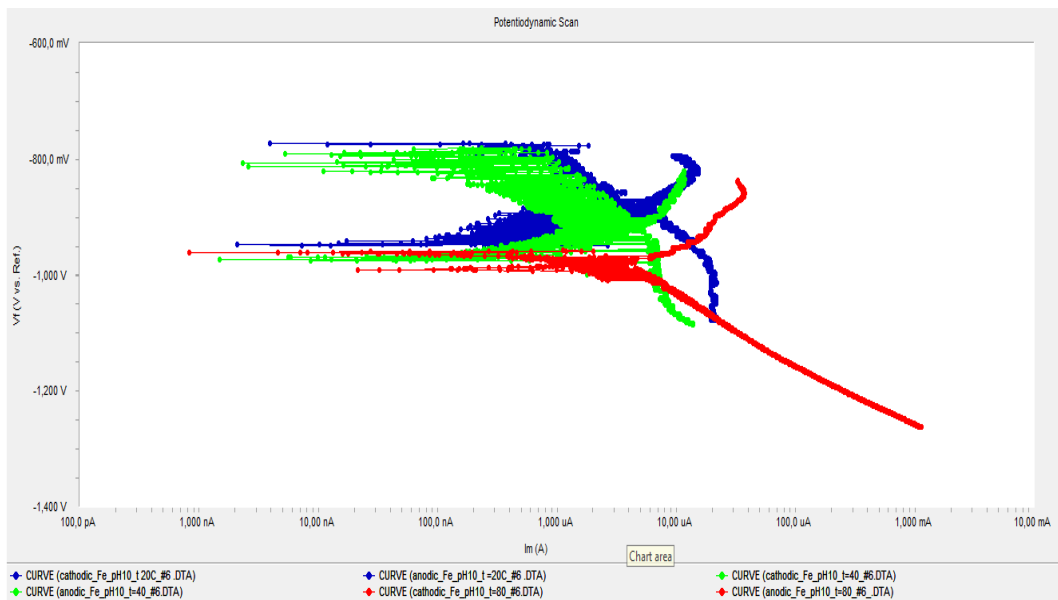


**Figure 30.** Potentiodynamic sweeps for covered with elemental sulfur working electrode at pH7 at 20°C (blue), 40°C (green), 80°C (red) after 24 hours.

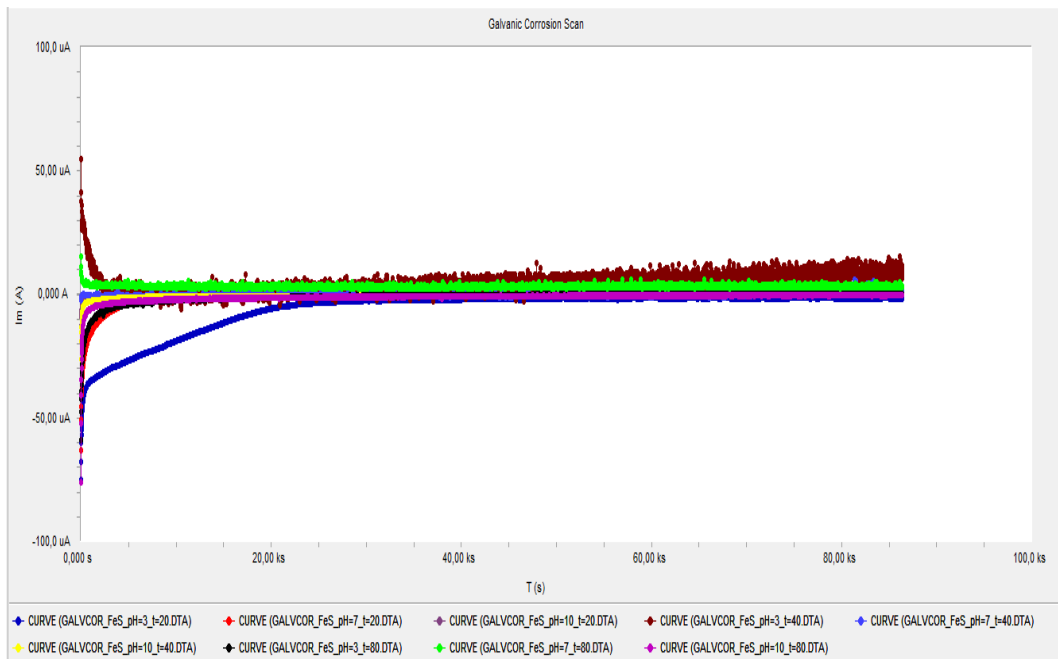


**Figure 31.** Potentiodynamic sweeps for covered with elemental sulfur working electrode at pH10 at 20°C (blue), 40°C (green), 80°C (red) after 24 hours.

The potentiodynamic scans for bare steel electrode were carried out after polarization sweeps of covered electrode. The more disturb oscillations took place during measurements. It was not possible to read clear information of polarization steps (Figure 32). To determine the possible cause of problem setup was assembled every time the noise was present. Working electrode was tested in three-electrode cell with electrolyte. The polarization sweep was carried out without any evidence of deviation. Reference electrode was tested with ammeter. Also the test of counter electrode was carried out. Inspection showed no problems with equipment. It is mean that the problem was with local electronic environment or chemistry. The chemistry problem is more likely. Electrochemical oscillations can result from either electrochemical or purely chemical origins. An electrochemical oscillation is dependent on the interfacial potential while a purely chemical oscillator is not [40]. During the polarization scans the anodic potential was in a range of -675 to -990 mV (SCE) (Figure 3 in appendix 2). Such a low values could be a reason of the oscillations. The sours of distortion should be investigated further.



**Figure 32.** Potentiodynamic sweeps for bare working electrode at pH3 at 20°C (blue), 40°C (green), 80°C (red) after 24 hours.



**Figure 33.** Galvanic corrosion scans for Fe/FeS couple in Series 2.

Figure 33 plots the galvanic corrosion measurements in Series 2. It can be clearly seen that tow curves have positive going scan under the conditions of pH7 at 80°C and pH3 at 40°C. This indicates that the iron sulfide-covered electrode was forced to corrode by bare electrode in galvanic coupling. Rest curves showed negative current values at the start of the test. The overview of the final current values is given in Table 8.

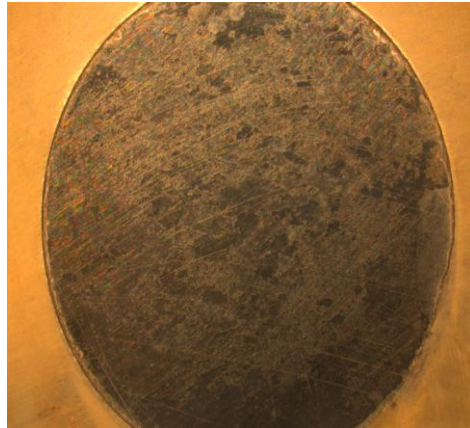
**Table 8.** Galvanic current for covered electrode in coupling Fe/FeS ( $\mu\text{A}$ ).

| Temperature | pH3    | pH7   | pH10   |
|-------------|--------|-------|--------|
| 20          | -1.581 | 0.958 | 19.57  |
| 40          | 15.57  | 2.103 | -0.355 |
| 80          | 0.110  | 4.98  | -0.430 |

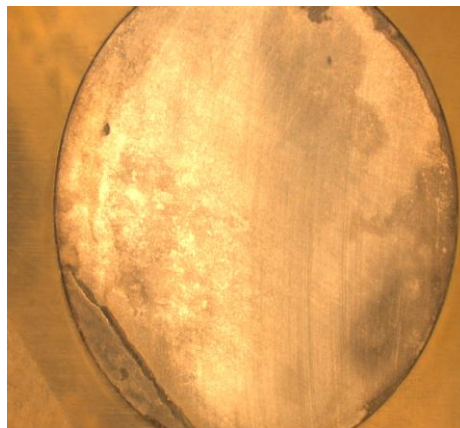
These results indicate that at the pH3 at 20°C, pH10 at 40°C and pH10 at 80°C negative going scan appeared over a period of test. In other experiments current became positive after first 3-5 hours. It was concluded that covered electrode will be corroded. After all test the pictures of electrodes were taken. Figure 2 in Appendix 2 shows no presence of corrosion on the surface of covered electrodes. Surface of bare steel electrode in all tests was covered with thin black layer. Only in two tests at pH7 at 40°C and pH10 at 40°C the evidence of general corrosion was observed while the surface of covered electrode remained metallic bright under the iron sulfide. These results are not contradict the OCP measurements (Figure 8) which showed that almost in all cases the bare electrodes had lower potential and acted as anode. But in the same moment the data obtained during galvanic corrosion scan shows opposite behavior of bare steel electrode. The reason for this may be that during Rp/Ec trend the electrodes were decoupled and the bare electrode corroded freely without any effect of covered electrode. After 24 hours of test running the iron sulfide-covered electrode started to corrode not significantly and bare electrode was protected by thin film from



further corrosion (Figure 34). The pictures of the covered electrode show that the corrosion products were mostly generated at the periphery of the iron sulfide pellet [41] uncovered with the Teflon tape (Figure 35). The corrosion type in this region is crevice and it could be a reason of positive current values for iron sulfide- covered electrode during galvanic corrosion scan.



**Figure 34.** Surface of bare carbon steel electrode at pH7 at 80°C.



**Figure 35.** Surface of covered (FeS) electrode at pH7 at 80°C after black film has been removed.

Results from the study of carbon steel covered with iron sulfide showed that the surface of electrode remained protected against the corrosion compared to elemental sulfur-covered electrode even at high pH and high temperature. Whereas the surface of sulfur-covered steel protected with thick film suffered with pitting corrosion. The process could be accelerated by presence of chloride played an important role in the corrosion process and indicated that electrochemical reactions may underpin elemental sulfur corrosion [23].

## 6 CONCLUSIONS

From the experiments performed on carbon steel X65 with elemental sulfur and iron sulfide as film formation agents coupled galvanically to similar metals, the following conclusions can be made:

- In galvanic coupling between two similar metals, the covered electrode was protected by corrosion products film from general corrosion. This trend was obtained even at low pH and high temperature.
- The corrosion type of covered electrode changed from general to localized/pitting with increase of temperature.
- The corrosion rate in general was high for lower pH and high temperature.
- In the cases with elemental sulfur-covered electrode, the presence of localized corrosion was obtained on covered electrode and bare electrode had general corrosion.
- In the cases with iron sulfide-covered electrode, the corrosion products protective layer was loose and cracked easily compared to elemental sulfur tests. After removal of the film surface of covered electrode remained metallic bright with no evidence of corrosion attack.

## 7 RECOMMENDATIONS AND FUTURE WORK

Because of the short term of the projects, the many questions related to the topic remained open. The following recommendations could be taking into consideration for future work

- The more accurate adjustment and monitoring of pH level.
- The different way to hold on the sulfur or iron sulfide powder on the surface of studied electrode, which could easier provide the access of electrolyte.
- The extending of the tests period.
- Further study of weight loss and analysis of corrosion products composition with study of morphology of the coupons surface and film thickness could be done.

## REFERENCES

1. J. Kvarekal, Morphology of Localized Corrosion Attacks in Sour Environments, NACE, Corrosion 2007, Paper No.07659.
2. Metals Handbook, Ninth Edition, Vol.11, Failure Analysis & Prevention, ASM International, 1986, Paper No. 298.
3. R.N.Tuttle, Guideline Aid in Designing for H<sub>2</sub>S Service, H<sub>2</sub>S Corrosion in Oil & Gas Production – A Compilation of Classic Paper, 1981, Paper No. 1077.
4. X.L. Cheng, H.Y. Ma, J.P. Zhang, X. Chen, S.H. Chen, and H.Q. Yang, Corrosion of Iron in Acid Solutions with Hydrogen Sulfide.
5. Sulfide Stress Cracking Resistant Metallic Materials for Oilfield Equipment, Standart MR0175-88, NACE, Houston (1988).
6. R.N. Tuttle, What Is a Sour Environment? , SPE, Tuttle & Assocs, 1990.
7. A.N. Cavallaro, Overview of H<sub>2</sub>S Souring Cases in Argentina Reservoirs: Origin and Mitigation Sceneries, SPE 107376, 2007.
8. N. Lukachenko, P. Bourges et al, Recent experience on sour service resistant steels behavior, NACE, Corrosion 2009, Paper No.09352.
9. J. W. Wallace, R.V. Reddy, D.V. Pugh, Sour Service Pit Growth Prediction of Carbon Steel Using Extreme Value Statistics, NACE 2007, Paper No. 07657.
10. R.V. Reddy, J.L. Pacheco, Accurate Corrosion Prediction through an Integrate Approach, IPTC 10675. Doha, Qatar, 2005.
11. NORSOK standard M-001, Materials selection, Rev. 4, August 2004.
12. J. B. Sardisco and R. E. Pitts, "Corrosion of Iron in an H<sub>2</sub>S - CO<sub>2</sub> - H<sub>2</sub>O System", Corrosion 21 (1965), Paper No. 350.
13. J. Amri, J. Kvarekvål, Simultation of Solid state Growth of Iron Sulfide in Sour Corrosion Conditions, NACE, 2011, Paper No. 11078.
14. W. Sun, Kinetics of iron carbonates and iron sulfide scale formation in CO<sub>2</sub>/H<sub>2</sub>S corrosion, 2006.

15. H. Fang, D. Young and S. Nesi, Elemental sulfur corrosion of mild steel at high concentration of sodium chloride, NACE International, 2009, Paper No. 2592.
16. Z. Zhu, Ph.D., EIT, N. Tajallipour, Ph.D., EIT, Patrick J. Teevens, CD, P.Eng., MCIC, Modeling of Elemental Sulfur Deposition in Sour-Gas Petroleum Pipelines, NACE, Corrosion 2011, Paper No. 11124.
17. G. Schmitt, "Present Day Knowledge of the Effect of Elemental Sulfur on Corrosion in Sour as Systems", Corrosion/90, Paper No. 39, Houston, TX NACE (1990).
18. D. D. MacDonald, B. Roberts, J. B. Hyne, "The Corrosion of Carbon Steel by Wet Elemental Sulfur, Corrosion Science 18 (1978) 411.
19. J. S. Smith, J. D. A. Miller, "Nature of Sulfides and Their Corrosive Effect on Ferrous Metals: A Review," Brit. Corrosion J. 10, 3 (1975).
20. S. Smith, J. Pacheco, "Prediction of Corrosion in Slightly Sour Environments," Corrosion 2002, Paper No. 241 (Houston, TX: NACE, 2002).
21. D. Abayarathna, A. Naraghi, N. Obeyesekere, Inhibition of Corrosion of Carbon Steel in the presence of CO<sub>2</sub>, H<sub>2</sub>S and S, Corrosion 2003, Paper No. 03340.
22. R. Steudel, "Mechanism for the Formation of Elemental Sulfur from Aqueous Sulfide in Chemical and Microbiological Desulfurization Processes", Industrial Engineering & Chemistry, Research, 1996, 35, 1417-1423.
23. H. Fang, B. Brown, D. Young, S. Nesi, Investigation of Elemental sulfur Corrosion Mechanisms, NACE Corrosion 2011, Paper No. 11398.
24. L. Zhang, W. Zhong, J. Yang, T. Gu, X. Xiao, and Minxu, Effects of Temperature and Partial Pressure on H<sub>2</sub>S/CO<sub>2</sub> Corrosion of Pipeline Steel in Sour Conditions, Corrosion 2011, Paper No. 11079.
25. W. Sun and S. Nesi, A Mechanistic Model of H<sub>2</sub>S Corrosion of Mild Steel, Corrosion 2007, Paper No. 07655.
26. R. C. John, A. L. Young, New Understanding on Corrosion of Alloys in High-Temperature Sulfidizing Gases, Corrosion 2002, Paper No. 02486.

27. D.W Shoemsmith, et al., The Formation of Ferrous Monosulfide Polymorphs during the Corrosion of Iron by Aqueous Hydrogen Sulfide at 210C. Electrochemical Society, 1980, Paper No. 1007-1015.
28. Z.A. Forouli, Electrochemical behavior and corrosion of iron in aqueous sulfidic solution, Werkstoffe and Korrosion, 1980, pp 463-470.
29. W. F. Rogers, J.A. Rowe Jr, Corrosion Effects Of Hydrogen Sulfide and Carbon Dioxide in Oil Production, Proceeding 4<sup>th</sup> World Petroleum Congress-Section II/G, Paper 3.
30. Gamry Instrument,  
[http://www.gamry.com/App\\_Notes/DC\\_Corrosion/GettingStartedWithEchemCorrMeasurements.htm](http://www.gamry.com/App_Notes/DC_Corrosion/GettingStartedWithEchemCorrMeasurements.htm).
31. D.G. Enos, The Potentiodynamic Polarization Scan, Technical report 33, 1997.
32. Materials Evaluation and Engineering, Inc., 2009.
33. S. Ewing, Electrochemical Studies of the Hydrogen Sulfide Corrosion Mechanism, South Central Regional Meet. NACE, Tulsa, Oklahoma, Oct., 1953 (Unpublished).
34. T. Hemmingsen, N. Aagotnes, T. Havn, Characterisation of sulphur compounds and examination of their effects with respect to corrosion, 2004
35. M. Pourbaix, "Atlas of Electrochemical Equilibria in Aqueous Solutions," NACE-Cebelcor, 1974.
36. C. Mendez, C. Scott, Laboratory Evaluation and Modeling of API-L80/13CR Galvanic Corrosion in CO2 Environment, NACE 2008, p.08325.]
37. J. Tang, Y. Shao, Corrosion Behavior of Carbon Steel in Different Concentration of HCl solution containing H<sub>2</sub>S at 90°C, Elsevier, Corrosion Science 53, 2011
38. Dr. P. Peterson, Gamry instruments, NACE presentation.
39. L. Zhang, Z. Wen et al, Effect of Deposition Characteristic and temperature on Elemental Sulfur Corrosion, NACE Corrosion 2011, Paper No. 11121.
40. K. Krischer , in: Alkire R.C. (Ed.), Advances in Electrochemical Science and Engineering, vol. 8, Wiley-VCH Verlag GmbH & Co, 2002.

41. H. Fang, D. Young and S. Nesie, Elemental Sulfur Corrosion of Mild Steel at High Concentration of Sodium Chloride, NACE International, 2009, Paper No.2592.



## APPENDIX 1

### Ståldata

Stål nr:

|                     |                                   |             |   |
|---------------------|-----------------------------------|-------------|---|
| Legering            | <input type="text" value="X-65"/> | Form        | <input ,="" 31,0"="" type="text" value="Rør 36" wt=""/> |
| Sveis               | <input type="text"/>              | Leverandør  | <input type="text" value="Shell"/>                      |
| Prosjekt            | <input type="text"/>              | Lagingssted | <input type="text" value="PT-2 kjeller plass 1.7"/>     |
| Prosjekt betegnelse | <input type="text"/>              | Beholdning  | <input type="text" value="Mer enn 3 kg"/>               |

#### Legeringselementer - grunnmateriale

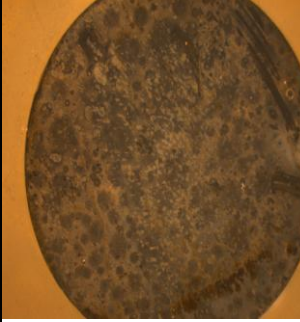

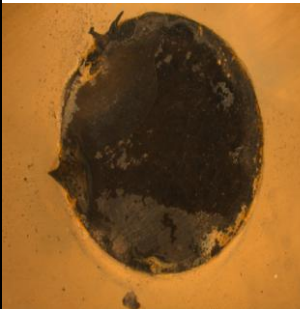


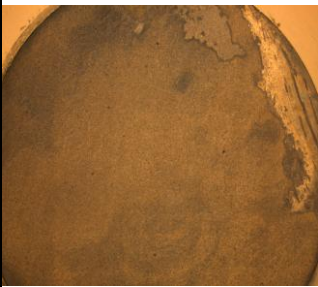

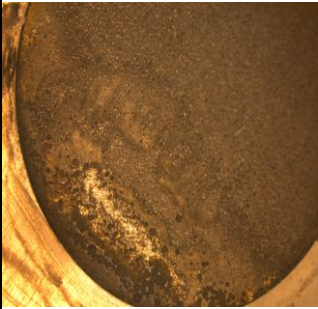
| C:   | Si:  | Mn:  | S:    | P:    | Cr:  | Ni:  | V:    | Mo:  | Cu:  | Al:   | Sn:   | Nb:   |
|------|------|------|-------|-------|------|------|-------|------|------|-------|-------|-------|
| 0.08 | 0.25 | 1.54 | 0.001 | 0.019 | 0.04 | 0.03 | 0.045 | 0.01 | 0.02 | 0.038 | 0.001 | 0.043 |

Mikrostruktur

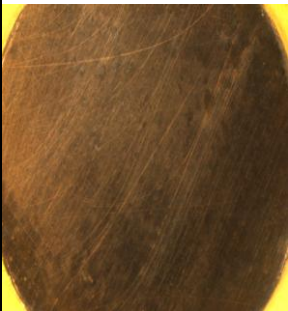

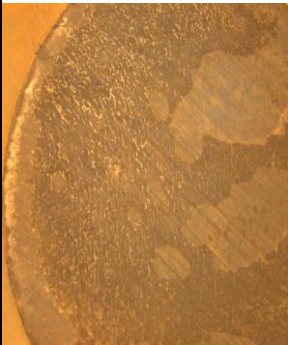

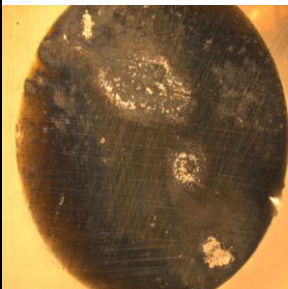
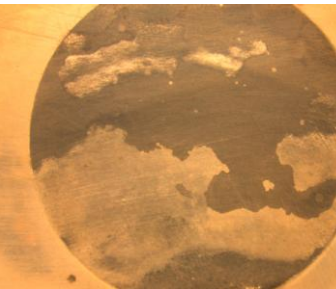
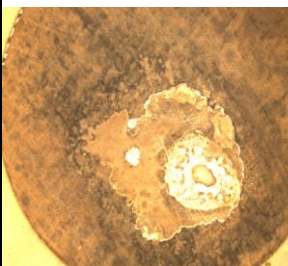
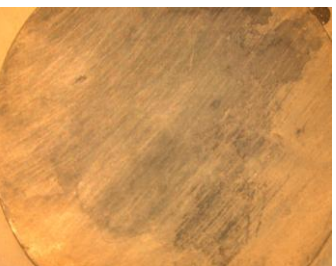
En bit fra Troll-ledningen

**Figure 1.** Certificate of carbon pipeline steel X65

**APPENDIX 2**

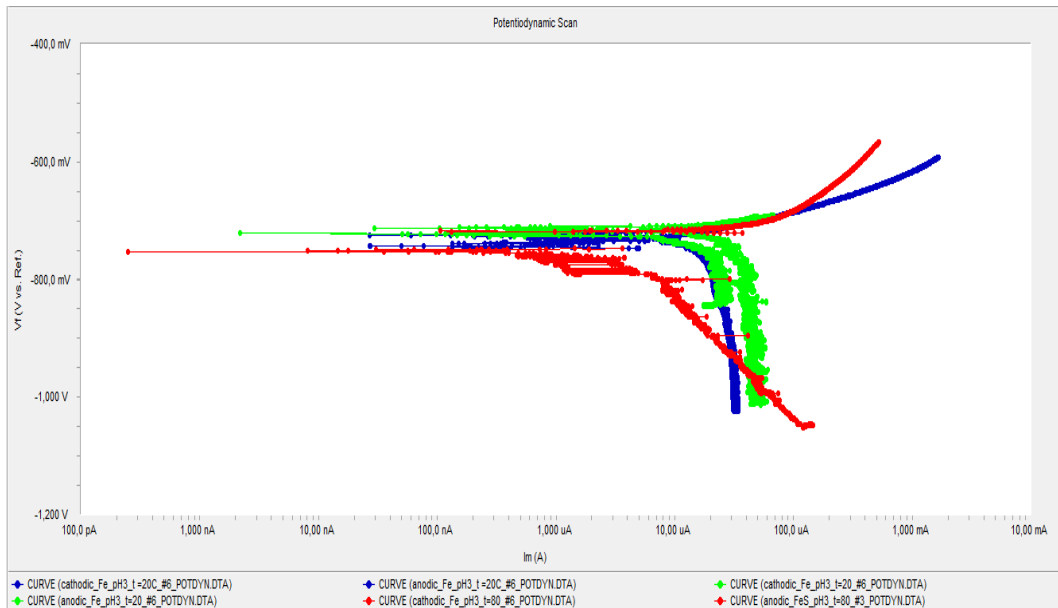
|              | Bare steel (Fe)  | Covered steel with sulfur (Fe+S)   | Description   |
|--------------|--|--|---|
| pH 3 at 80°C | 1<br>   | 2<br>   | 1). Presence of thick black film, local corrosion traces;<br>2). Thick black film, general corrosion traces.  |
|              | 3<br>  | 4<br>  | 3). Thin black film, easily to remove, general corrosion;<br>4). Thick black film, general corrosion traces.  |
| pH 7 at 20°C | 5<br> | 6<br> | 5). Thin black film, under the film metal remained metallic bright, steel suffered local corrosion;<br>6). Thick black film, presence of localized corrosion in non-covered region, several pits. |
|              | 7<br> | 8<br> | 7). Thick black film, surface suffered with localized corrosion;<br>8). Thick black film, presence of pitting corrosion in non-covered region and near.   |

**Figure 1.** Morphology of steel surface of bare and covered electrodes in Series 1.

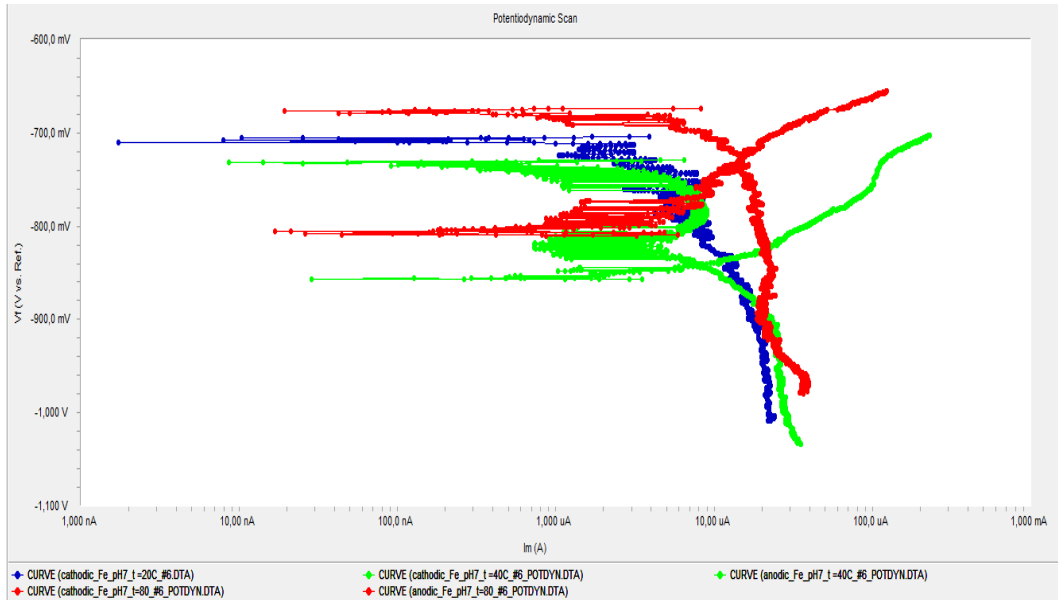
|               | Bare steel (Fe)  | Covered steel iron sulfide (FeS)   | Description  |
|---------------|--|--|--|
| pH10 at 80°C  | 1<br>   | 2<br>   | 1). Thin black film, hard to remove, no evidences of changes due to corrosion;<br>2). Thin black film, after removal, evidences of localized corrosion, surface darkened slightly. |
|               | 3<br>  | 4<br>  | 3). No black film on the surface, traces of localized corrosion;<br>4). Thick black film, after removal the surface slightly darkened, no evidence of corrosion attack.            |
| pH 10 at 40°C | 5<br> | 6<br> | 5). Thin black film, hard to remove, traces of localized corrosion;<br>6). Thin black film, non-adherent and cracks easily, no evidence of corrosion attack.                       |
|               | 7<br> | 8<br> | 7). Thin black film, localized corrosion;<br>8). Thin black film, non-adherent and cracks easily, surface under film slightly darkened, no evidence of corrosion attack.           |

**Figure 2.** Morphology of steel surface of bare and covered electrodes in Series 2.

**Polarization sweeps for bare electrode (galvanic couple Fe/FeS) after 24 hours (Series 2).**



a).



b).

**Figure 3.** The potentiodynamic sweeps for bare working electrode after 24 hours: a) pH3, b) pH7, at 20°C (blue), 40°C (green), 80°C (red).